THIS DOCUMENT PROVIDED BY THE ABBOTT AEROSPACE
TECHNICAL LIBRARY
ABBOTTAEROSPACE.COM

C.P. No. 1358

C.P. No. 1358

PROCUREMENT EXECUTIVE, MINISTRY OF DEFENCE

AERONAUTICAL RESEARCH COUNCIL

CURRENT PAPERS

A Practical Approach to the Prediction of Oscillatory Pressure Distributions on Wings in Supercritical Flow

LIBRARY
ESTABLISHMENT
R.A.E.
BEDFORD.

by

H. C. Garner

Aerodynamics Dept., R.A.E., Farnborough

LONDON: HER MAJESTY'S STATIONERY OFFICE

1976

£2-20 NET

THIS DOCUMENT PROVIDED BY THE ABBOTT AEROSPACE
TECHNICAL LIBRARY
ABBOTTAEROSPACE.COM

UDC 533.693 : 533.6.013.422 : 533.6.048.2 : 533.6.011.35 : 533.693.9

*CP No.1358
December 1974

A PRACTICAL APPROACH TO THE PREDICTION OF OSCILLATORY PRESSURE DISTRIBUTIONS ON WINGS IN SUPERCRITICAL FLOW

by

H. C. Garner

SUMMARY

Brief consideration of current approaches to the prediction of unsteady wing loading in mixed subsonic and supersonic flow shows a wide variety of method and a clear need for economy in transonic aerodynamic calculations for flutter clearance in subsonic flight. In support of measurements of steady and oscillatory pressure distributions on a particular wing, an approximate theoretical treatment is devised in terms of non-linear steady surface pressures and linear oscillatory loading. The steady data are taken either from transonic small-perturbation theory or from the static experiments. The resulting theoretical or semi-empirical calculations can take account of stream Mach number, mean incidence, mode of oscillation, frequency and amplitude. Like the dynamic experiments, the theoretical and semi-empirical results show large differences between oscillatory chordwise load distributions under subcritical and supercritical conditions, especially in the recompression region where the large and rapidly changing amplitude and phase of the measured loading are reproduced qualitatively in the calculations. The method should provide an economical indication of the importance of non-linear flutter aerodynamics in the lower transonic regime.

---

* Replaces RAE Technical Report 74181 - ARC 36100

THIS DOCUMENT PROVIDED BY THE ABBOTT AEROSPACE
TECHNICAL LIBRARY
ABBOTTAEROSPACE.COM

CONTENTS

THIS DOCUMENT PROVIDED BY THE ABBOTT AEROSPACE
TECHNICAL LIBRARY
ABBOTTAEROSPACE.COM

1 INTRODUCTION

The achievement of satisfactory flutter characteristics in aircraft design depends mainly on aeroelastic calculation, sometimes supplemented by a limited amount of flutter testing in wind tunnels. The present inquiry into unsteady transonic flow has been prompted particularly by current interest in the 'supercritical wing' - the type of wing designed to exploit mixed subsonic and supersonic flow over its upper surface. There is a special need to examine and eliminate, if necessary, any undesirable features in the flutter behaviour of a wing under these conditions. A combined theoretical and experimental study of oscillatory pressure distributions has therefore been undertaken for a wing design that would in practice operate with some degree of supercritical flow. A preliminary account of the investigation has appeared in Ref.1. The experimental results are being reported more fully by Lambourne and Welsh in Ref.2, which discusses the physical processes involved and their significance in relation to flutter. In the present paper the theoretical content of Ref.1 is presented more directly with fewer approximations and is illustrated both with and without its empirical element.

2 THEORETICAL BACKGROUND

2.1 Linearized theories

By 'linearized theory' or 'linear theory' in this Report we imply a method of calculation in which wing thickness is ignored and, moreover, the displacements of the wing from a streamwise plane and the perturbations of a uniform potential flow are considered only to first order. Such methods are to be distinguished from those which consider small perturbations of some known steady flow past a wing of finite thickness or displacement.

At purely subsonic or supersonic speeds, satisfactory methods of representing the unsteady aerodynamics in aeroelastic calculations have been developed with neglect of aerofoil thickness. The available methods are too numerous to mention, but on the subsonic side it is useful to distinguish between the kernel-function methods such as Ref.3 and the doublet-lattice methods such as Ref.4. While most subsonic methods are general in planform, frequency and Mach number, in supersonic flow it is often necessary to impose conditions on such parameters; however, the refined box-method of Allen and Sadler[5] has minimal restrictions of this kind. The intervening transonic speed range can be bridged with the aid of the sonic theories of Landahl[6] and Davies[7]. Thus the present author and

This Document Provided by the Abbott Aerospace
TECHNICAL LIBRARY
ABBOTTAEROSPACE.COM

Miss Lehrian[8] have produced linearized theoretical data on the pitching derivatives of selective planforms over a range of frequency parameter as continuous curves against Mach number. While the supporting experimental evidence shows some qualitative resemblance, it has become clear that the purely theoretical transonic effects revealed in Ref.8 are of academic rather than practical interest. The use of linearized theory imposes such increasingly severe restrictions on wing thickness, mean incidence and amplitude of oscillation as sonic Mach number is approached that practical applications tend to avoid the range between 0.8 and 1.2, say, where the real flutter derivatives have often been regarded as unpredictable. The only expedient is then to estimate the intermediate flutter characteristics from faired curves between the subsonic and supersonic regimes. In the absence of related experimental justification such a procedure may be no more realistic than linearized theory itself.

In calculations of steady pressure distributions for the purpose of wing design it is imperative to incorporate the influence of aerofoil thickness and to make allowance for the boundary layer and wake. In most flutter calculations, however, these complications are either ignored or treated by means of empirical modifications to linearized theory. For example, the corrective matrix method of Ref.9 is sometimes used to adjust the results of linearized theory in accord with oscillatory experimental data for one single mode, with application to arbitrary modes throughout the flutter analysis. While this technique has succeeded in subcritical flow, it must become problematical under supercritical conditions.

2.2 Non-linear theories

Whereas the linearized aerodynamic problem can be defined in terms of planform, modes of oscillation, frequency and Mach number, there are other parameters to consider under conditions of mixed subsonic and supersonic flow. The oscillatory content of the resulting flow can no longer be regarded as independent of wing thickness, wing camber and mean incidence. While the most salient feature of the mean flow is the sonic line or the location of embedded shock waves, this is but one characteristic of the steady flow to be perturbed, which needs to be defined in terms of the distribution of surface pressure or local Mach number. Reynolds number and amplitude of oscillation are two further parameters that are likely to be important; both call for treatment semi-empirically or otherwise.

THIS DOCUMENT PROVIDED BY THE ABBOTT AEROSPACE
TECHNICAL LIBRARY
ABBOTTAEROSPACE.COM

Various attacks on the problem of transonic unsteady aerodynamics are reported in the recent literature. In a brief review of current theoretical work sponsored by the NASA Langley Research Center, Bland[10] considers several methods of analysis. Tijdeman and Zwaan[11] discuss the requirements of such methods in more detail. Broadly these methods fall into three categories

(i) finite-difference methods,

(ii) lifting-surface-element methods,

(iii) more specialized methods.

The finite-difference methods can be regarded as extensions of the treatment of two-dimensional steady transonic flow by Murman and Cole[12], who use a relaxation technique based on central differences at subsonic points and upstream differences at supersonic points. The most promising of the developments in Ref.10 appears to be the finite-difference method of Ehlers[13], which is reported as having been used with some success for three-dimensional surfaces in steady flow; it is further stated in Ref.10 that the analysis for three-dimensional unsteady flow has been developed, but not yet programmed. At the Royal Aircraft Establishment on similar lines Albone, *et al.*[14] have developed a method for two-dimensional steady flow, which has recently been extended to wings of arbitrary planform[15]; results from this latter method are used in some of the present calculations. It is difficult to assess the long-term prospect of realizing a general theoretical method for unsteady flow, but there is little doubt that the routine use of a finite-difference method would be very expensive.

The lifting-surface-element methods provide solutions at lower cost. The general approach is to subdivide the upper and lower surfaces into regions associated with different stream Mach numbers derived from the mean flow. One method on these lines is presented and discussed with examples by Cunningham[16]. Although his method is not fully developed, it offers a significant improvement on linearized theory. The solutions are obtained with a constant supersonic stream Mach number ahead of the shock wave and a constant subsonic one behind it. Another method in this category is propounded in Ref.11 and applied successfully when the flow is just subcritical. There are, however, some basic differences between them. While Ref.16 uses the kernel-function method, Ref.11 uses the doublet-lattice method with a different stream Mach number for each panel: both methods use the prescribed stream Mach number in the local boundary condition but, while in Ref.16 it is also used to compute the neighbouring downwash field, in Ref.11 the downwash field of each panel corresponds to the average of its

THIS DOCUMENT PROVIDED BY THE ABBOTT AEROSPACE
TECHNICAL LIBRARY
ABBOTTAEROSPACE.COM

local Mach number and the true stream Mach number. Either method provides numerical results in a time comparable with that of the appropriate linearized solution.

Three other contrasting methods are discussed in Ref.10. The local-linearization procedure of Stahara and Spreiter[17] is strictly for a sonic stream Mach number and is probably unsuitable for a typical supercritical flow when the stream Mach number is below 0.9 and the local Mach number may range at least from 0.7 to 1.3. The layered-medium analysis of Revell[18] uses strata of different uniform supersonic Mach number within the region of two-dimensional supercritical flow; it is questionable whether such a method could be extended into three dimensions. Finally there is the modified sonic-box method of Ruo and Theisen[19] which, like Ref.17, is too restrictive in Mach number to cover supercritical flow as a whole.

The increasing scale of current effort being devoted to the problem of unsteady supercritical flow is evidence, not only of concern among flutter specialists, but of confidence that rapid progress is round the corner. From the standpoint of intrinsic accuracy it may well be that the work of Ehlers[13] shows the greatest promise. But, on account of the vast computing effort involved in relaxation solutions by finite differences, this approach would be a formidable routine when conditions are so non-linear that each mean steady flow would require its own set of oscillatory perturbations. The economic argument against the use of the finite-difference technique is elaborated by Cunningham[16] and strengthens his case for the lifting-surface-element method. There is wide scope here, and it may take years of theoretical and experimental effort to establish the best assumptions. However, the framework of doublet-lattice elements, each associated with the local stream conditions as proposed in Ref.11, has logical generality and simplicity to commend it. A satisfactory extension of this method of calculation to mixed subsonic and supersonic flow is an attractive goal.

2.3 Practical approach

The present approach to the problem is explained in section 3. In the first place the mean steady pressure distribution is taken from a suitable source. To the steady velocity potential there is added a small oscillatory component dependent on the gradient with respect to incidence of the local steady pressure and also on the linearized subsonic theoretical values under the appropriate steady and oscillatory conditions. The unsteady velocity perturbation

THIS DOCUMENT PROVIDED BY THE ABBOTT AEROSPACE
TECHNICAL LIBRARY
ABBOTTAEROSPACE.COM

is then related to the unsteady pressure through Bernoulli's equation in one dimension. Whereas in Ref.1 the steady pressures and their gradients are taken from an initial experiment, the present calculations use the theory of Ref.15 and the newer static measurements of Ref.2 as alternative sources. The theoretical results provide a detailed illustration of the important influence of supercritical flow on the chordwise distribution of oscillatory pressures and give qualitative support to the dynamic measurements of Ref.2. In its semi-empirical form the method takes account of Reynolds number and admits the possibility to incorporate non-linear effects of the amplitude of oscillation through adjustment to the static gradients. Moreover, insofar as the oscillatory input to the calculation is treated to first order, the method has possible application to non-harmonic time-dependent flows such as occur in problems of gust entry.

3 APPROXIMATE THEORETICAL TREATMENT

It is considered that the development of a realistic mathematical model of three-dimensional unsteady supercritical flow, coupled with an economical method of solution, may prove to be a slow process. In the meantime the transonic regime, with all its uncertainties, continues to present a flutter hazard that demands appraisal at the earliest opportunity. The present approach is directed primarily to wings in a high subsonic main stream with embedded supersonic flow, and it is supposed that the distribution of steady surface pressure is known over a range of incidence. Knowledge of steady and oscillatory load distributions from subsonic linearized theory is also assumed. The objective is to formulate a useful approximation to the oscillatory pressure distribution from this combined information, which should normally be available when flutter clearance is sought.

The present application is to a wing of current design, the planform of which is shown in Fig.1; the measured static and dynamic pressures at the five stations (I to V) for oscillations about the swept axis $x = x_a$ are described in Ref.2. The model has camber and twist and a streamwise thickness-to-chord ratio of approximately 0.10. The incidence α is defined as that of the crank station $y = 0.319s$, relative to which the root and tip incidences are +3.93 and -0.57 degrees respectively. While our immediate purpose is to validate a method of calculation in the light of this particular experiment, the requirement is for a method of general applicability to enable the aircraft industry to anticipate any danger of wing flutter in supercritical flow. This could well be dependent on the steady aeroelastic deformation.

THIS DOCUMENT PROVIDED BY THE ABBOTT AEROSPACE
TECHNICAL LIBRARY
ABBOTTAEROSPACE.COM

3.1 Bernoulli's equation

We first derive a one-dimensional relationship between oscillatory velocity and pressure coefficient in compressible flow. The adiabatic law

$$p/\rho^{\gamma} = \text{constant} \tag{1}$$

and the equation for the local speed of sound

$$a = (\gamma p/\rho)^{\frac{1}{2}} \tag{2}$$

are considered to apply in steady and unsteady flow alike. It follows at once from equation (2) for the main stream (denoted by the subscript ∞) that the local unsteady pressure may be expressed as

$$p/p_{\infty} = 1 + \tfrac{1}{2}\gamma M_{\infty}^2 C_p \quad , \tag{3}$$

where the stream Mach number $M_{\infty} = U_{\infty}/a_{\infty}$ and the pressure coefficient

$$C_p = (p - p_{\infty})\Big/\left(\tfrac{1}{2}\rho_{\infty} U_{\infty}^2\right) \quad . \tag{4}$$

In time-dependent flow Bernoulli's equation is

$$\tfrac{1}{2}U^2 + \int \frac{dp}{\rho} + \frac{\partial \Phi}{\partial t} = \text{constant} \quad , \tag{5}$$

where Φ is the velocity potential. The velocity is written as

$$U(x,t) = U_0(x) + \frac{\partial}{\partial x}\left[\Re\left\{\bar{\Phi}(x)e^{i\omega t}\right\}\right] \quad , \tag{6}$$

where U_0 corresponds to the local mean flow, ω is the circular frequency of oscillation, and second-order terms in the complex velocity potential $\bar{\Phi}$ will be neglected. Thus, with the aid of equation (1), equation (5) becomes

$$\tfrac{1}{2}U_0^2 + \Re\left\{\left(U_0 \frac{d\bar{\Phi}}{dx} + i\omega\bar{\Phi}\right)e^{i\omega t}\right\} + \frac{\gamma p}{(\gamma - 1)\rho} = \tfrac{1}{2}U_{\infty}^2 + \frac{\gamma p_{\infty}}{(\gamma - 1)\rho_{\infty}} \quad , \tag{7}$$

whence by further use of equations (1) and (2)

THIS DOCUMENT PROVIDED BY THE ABBOTT AEROSPACE
TECHNICAL LIBRARY
ABBOTTAEROSPACE.COM

$$\frac{U_0^2}{U_\infty^2} - 1 + \frac{2}{U_\infty^2} \Re\left\{\left(U_0 \frac{d\bar{\Phi}}{dx} + i\omega\bar{\Phi}\right) e^{i\omega t}\right\}$$

$$= \frac{2}{(\gamma - 1)M_\infty^2}\left(1 - \frac{a^2}{a_\infty^2}\right) = \frac{2}{(\gamma - 1)M_\infty^2}\left[1 - \left(\frac{p}{p_\infty}\right)^{\frac{\gamma-1}{\gamma}}\right] . \qquad (8)$$

Elimination of p/p_∞ from equations (3) and (8) gives

$$\left(1 + \tfrac{1}{2}\gamma M_\infty^2 C_p\right)^{\frac{\gamma-1}{\gamma}} = 1 + \tfrac{1}{2}(\gamma - 1)M_\infty^2\left[1 - \frac{U_0^2}{U_\infty^2} - \frac{2}{U_\infty^2}\Re\left\{\left(U_0 \frac{d\bar{\Phi}}{dx} + i\omega\bar{\Phi}\right) e^{i\omega t}\right\}\right] . \qquad (9)$$

When equation (9) is expanded to first order in the time-dependent quantities, the pressure coefficient is obtained as

$$C_p = C_{p0} + \Re\left\{\bar{C}_p e^{i\omega t}\right\} , \qquad (10)$$

where

$$C_{p0} = \frac{2}{\gamma M_\infty^2}(G^\gamma - 1) , \qquad (11)$$

$$\bar{C}_p = -\frac{2G}{U_\infty^2}\left(U_0 \frac{d\bar{\Phi}}{dx} + i\omega\bar{\Phi}\right) \qquad (12)$$

with

$$G = \left\{1 + \tfrac{1}{2}(\gamma - 1)M_\infty^2\left(1 - \frac{U_0^2}{U_\infty^2}\right)\right\}^{\frac{1}{\gamma-1}} = \left(1 + \tfrac{1}{2}\gamma M_\infty^2 C_{p0}\right)^{\frac{1}{\gamma}} . \qquad (13)$$

It will now be assumed that equations (10) to (13) hold in three-dimensional flow. The velocity potential on the surface of the wing is written as

$$\Phi(x,y,t) = \Phi_0(x,y) + \Re\left\{\bar{\Phi}(x,y)e^{i\omega t}\right\} . \qquad (14)$$

The total derivative in equation (12) is replaced by the partial derivative, so that the oscillatory component of the surface pressure is given by

This Document Provided by the Abbott Aerospace
TECHNICAL LIBRARY
ABBOTTAEROSPACE.COM

$$\bar{C}_p = -\frac{2G}{U_\infty^2}\left(U_0 \frac{\partial \bar{\Phi}}{\partial x} + i\omega\bar{\Phi}\right) \quad . \tag{15}$$

This approximation ignores any influence of the lateral components of U_0 .

3.2 Oscillatory pressure distribution

We seek a plausible expression for $\bar{\Phi}$ to use in equation (15). As Appendix B of Ref.1 shows, the present method was originally conceived as an extension of the approximate formulation for steady incompressible flow in Ref.20. However, the argument in Ref.1 can be interpreted more directly; moreover, the approximation preceding equation (B-18) of Appendix B can be regarded as optional.

The oscillatory wing loading from subsonic linearized theory is written as the non-dimensional pressure difference

$$\Delta C_p = C_{p\ell} - C_{pu} = \ell_0 + \mathcal{R}\left\{\bar{\ell} e^{i\omega t}\right\} \quad , \tag{16}$$

where $C_{pu} = -C_{p\ell}$ and

$$\bar{\ell} = \frac{8s}{\pi c(\eta)} e^{-i\omega x/U_\infty} \sum_{q=1}^{N} \bar{\Gamma}_q(\eta) \frac{\cos(q-1)\phi + \cos q\phi}{\sin\phi} \tag{17}$$

may be calculated from a numerical solution by the method of Ref.3 for the required modes of oscillation. Here N denotes the number of chordwise terms in the solution, $\bar{\Gamma}_q$ is a complex function of $\eta = y/s$ proportional to the amplitude of oscillation, and ϕ is related to the local chordwise position

$$\xi = \frac{x - x_L(\eta)}{c(\eta)} = \tfrac{1}{2}(1 - \cos\phi) \quad . \tag{18}$$

The linearized form of equation (15), with $U_0 = U_\infty$, is

$$\frac{\partial \bar{\Phi}_{lin}}{\partial x} + \frac{i\omega\bar{\Phi}_{lin}}{U_\infty} = \pm \tfrac{1}{4} U_\infty \bar{\ell}(x,\eta) \quad , \tag{19}$$

THIS DOCUMENT PROVIDED BY THE ABBOTT AEROSPACE
TECHNICAL LIBRARY
ABBOTTAEROSPACE.COM

where the symbol $\pm$ denotes positive for the upper surface and negative for the lower surface. This linear differential equation is readily solved to give

$$\bar{\Phi}_{lin} = \pm e^{-i\omega x/U_\infty} \int_{x_L}^{x} \tfrac{1}{4}U_\infty \bar{\ell}(x',\eta) e^{i\omega x'/U_\infty} dx'$$

$$= \pm \tfrac{1}{4}U_\infty \bar{c}\bar{I} e^{-i\omega x/U_\infty} , \qquad (20)$$

where the geometric mean chord $\bar{c}$ is taken as reference length and

$$\bar{I} = \frac{1}{\bar{c}} \int_{x_L}^{x} \bar{\ell}(x',\eta) e^{i\omega x'/U_\infty} dx'$$

$$= \frac{4s}{\pi \bar{c}} \left[\bar{\Gamma}_1(\eta)(\phi + \sin\phi) + \sum_{q=2}^{N} \bar{\Gamma}_q(\eta) \left(\frac{\sin(q-1)\phi}{q-1} + \frac{\sin q\phi}{q} \right) \right] . \qquad (21)$$

Hence

$$\frac{\partial \bar{\Phi}_{lin}}{\partial x} = \pm \tfrac{1}{4}U_\infty \left[\bar{\ell} - i\bar{\nu}\bar{I} e^{-i\bar{\nu}x/\bar{c}} \right] = \pm \tfrac{1}{4}U_\infty \bar{K} , \quad \text{say} , \qquad (22)$$

where $\bar{\nu} = \omega\bar{c}/U_\infty$ is the frequency parameter.

For the purposes of the approximate treatment we simply assume that

$$\frac{\partial \bar{\Phi}/\partial x}{(\partial \bar{\Phi}/\partial x)_{\bar{\nu}=0}} = \left[\frac{\partial \bar{\Phi}/\partial x}{(\partial \bar{\Phi}/\partial x)_{\bar{\nu}=0}} \right]_{lin} = \frac{\bar{K}}{(\bar{\ell})_{\bar{\nu}=0}} . \qquad (23)$$

Since by equation (15)

$$(\partial \bar{\Phi}/\partial x)_{\bar{\nu}=0} = -\frac{U_\infty^2}{2GU_0} (\bar{C}_p)_{\bar{\nu}=0} , \qquad (24)$$

equation (23) becomes

THIS DOCUMENT PROVIDED BY THE ABBOTT AEROSPACE
TECHNICAL LIBRARY
ABBOTTAEROSPACE.COM

$$\frac{\partial \bar{\Phi}}{\partial x} = -\frac{U_\infty^2 \bar{K}}{2GU_0}\left(\frac{\bar{C}_p}{\bar{\ell}}\right)_{\bar{\nu}=0} . \tag{25}$$

Therefore by equations (15) and (25) the oscillatory chordwise pressure distribution on the upper or lower surface is given by

$$\bar{C}_p(\xi) = \bar{K}(\xi)\left(\frac{\bar{C}_p(\xi)}{\bar{\ell}(\xi)}\right)_{\bar{\nu}=0} + \frac{i\bar{\nu}cG(\xi)}{\bar{c}}\int_0^{\xi}\frac{\bar{K}(\xi')U_\infty}{G(\xi')U_0(\xi')}\left(\frac{\bar{C}_p(\xi')}{\bar{\ell}(\xi')}\right)_{\bar{\nu}=0} d\xi' , \tag{26}$$

where $G(\xi)$ is defined in equation (13) in terms of the mean local pressure coefficient $C_{p0}(\xi)$.

The simpler result in equation (22) of Ref.1 can be derived from equation (26), if the correction factor multiplying $\bar{K}(\xi')$ in the integrand is replaced by its local value at $\xi' = \xi$. Hence we obtain the approximation

$$\bar{C}_p(\xi) = \left(\frac{\bar{C}_p}{\bar{\ell}}\right)_{\bar{\nu}=0}\left[\bar{K}(\xi) + \frac{i\bar{\nu}cU_\infty}{\bar{c}U_0}\int_0^{\xi}\bar{K}(\xi')d\xi'\right] , \tag{27}$$

which by means of equations (20) and (22) becomes

$$\bar{C}_p(\xi) = \left(\frac{\bar{C}_p}{\bar{\ell}}\right)_{\bar{\nu}=0}\left[\bar{\ell} - i\bar{\nu}\left(1 - \frac{U_\infty}{U_0}\right)\bar{I}e^{-i\bar{\nu}x/\bar{c}}\right] . \tag{28}$$

The relative merits of equations (26) and (28) will be discussed later.

In the present application to a rigid wing at mean incidence α_0 we can identify $(\bar{C}_p)_{\bar{\nu}=0}$ with $(\partial C_p/\partial\alpha)_0$ and $(\bar{\ell})_{\bar{\nu}=0}$ with $\partial\ell/\partial\alpha$ which is calculated by means of linearized subsonic lifting-surface theory[3] in the form of equation (17) without the exponential factor and with real coefficients Γ_q in place of $\bar{\Gamma}_q$. From equation (13) the velocity ratio

$$\frac{U_\infty}{U_0} = \left[1 - \frac{2}{(\gamma-1)M_\infty^2}\left\{\left(1 + \tfrac{1}{2}\gamma M_\infty^2 C_{p0}\right)^{\frac{\gamma-1}{\gamma}} - 1\right\}\right]^{-\frac{1}{2}} \tag{29}$$

THIS DOCUMENT PROVIDED BY THE ABBOTT AEROSPACE
TECHNICAL LIBRARY
ABBOTTAEROSPACE.COM

is obtained as a function of C_{p0} . Thus the evaluation of equation (26) or (28) at a spanwise station requires the knowledge of the chordwise distributions of C_p and $\partial C_p/\partial\alpha$ at the mean incidence α_0 in addition to the theoretical quantities in equations (17), (21) and (22). In the present calculations C_{p0} and the corresponding $\partial C_p/\partial\alpha$ have been taken from steady transonic theory[15] and from static measurements of Ref.2. Whereas the all-theoretical calculations of oscillatory pressures are presented and discussed in section 4.2 without appeal to experiment, the practical justification of the semi-empirical results receives detailed consideration in section 5.2.

In an application to flutter the interpretation of $(\bar{C}_p/\bar{\ell})_{\bar{\nu}=0}$ needs to be considered. While it could be argued that this should vary according to the mode of oscillation, it might suffice to retain the ratio corresponding to a rate of change of incidence for all modes. Such an assumption would be in the spirit of Ref.9 and, although unproven for supercritical flow, it might be the only practicable scheme if experimental data were used. It would be feasible to examine the ratio for each individual mode on the basis of transonic theoretical calculations. There is, however, the possibility that $(\bar{\ell})_{\bar{\nu}=0}$ may vanish locally, a difficulty that would not normally arise with $\partial\ell/\partial\alpha$.

4 USE OF TRANSONIC SMALL-PERTURBATION THEORY

Before we consider the transonic small-perturbation (TSP) theory of Ref.15 in section 4.1, it is well to recall Fig.5 of Ref.1 where in effect equation (28) has been used in conjunction with the approximate steady-flow theory of Ref.20 with linear corrections for compressibility. The oscillation about the swept axis $x = x_a$ of Fig.1 is expressed in terms of the instantaneous incidence

$$\alpha = \alpha_0 + \Re\left\{\alpha_1 e^{i\omega t}\right\} , \tag{30}$$

and the oscillatory chordwise loading is split into its real and imaginary parts so that

$$\bar{C}_{p\ell}(\xi) - \bar{C}_{pu}(\xi) = \Delta\bar{C}_p(\xi) = \Delta C_p' + i\Delta C_p'' . \tag{31}$$

Fig.5 of Ref.1 indicates that in subcritical flow the effect of wing thickness is not too important; the difference between the broken curves of $\Delta C_p'/\alpha_1$ reflects the influence of thickness in steady flow, while the chordwise distribution of $\Delta C_p''/\alpha_1\bar{\nu}$ shows much more dependence on frequency parameter than on

THIS DOCUMENT PROVIDED BY THE ABBOTT AEROSPACE
TECHNICAL LIBRARY
ABBOTTAEROSPACE.COM

thickness. It has since been verified that the use of equation (26) in place of equation (28) would make little material change. It is reasonable, therefore, to rely on linearized theory, such as Ref.3, for flutter calculations at sub-critical Mach numbers provided that the lift is a linear function of incidence.

Under transonic conditions, however, the quantity

$$\left(\frac{\bar{C}_p}{\bar{\ell}}\right)_{\bar{\nu}=0} = \frac{(\partial C_p/\partial\alpha)_0}{\partial\ell/\partial\alpha} \qquad (32)$$

can be expected to play a dominant rôle. Although counter arguments are made in section 5, there are the following advantages in determining the numerator from TSP theory rather than experiment. In the first place C_p is available at more chordwise positions, which can be chosen to give adequate definition over the whole chord and to facilitate the integration in equation (26): secondly, the differentiation with respect to α is not blurred by experimental scatter. Moreover, the theoretical calculations of section 4.2 should provide a better yardstick than those from subsonic lifting-surface theory, whereby to assess the dynamic measurements of Ref.2. In the early design stage only the theory may be sufficiently complete to provide the necessary data.

4.1 Steady flow

The three-dimensional TSP method of Albone, Hall and Joyce, which is featured in a survey by Lock, is still undergoing refinement. The computer program is expensive to run but, once a solution at one incidence for a given Mach number has been obtained, it is relatively quick to increase α in small stages.

A relaxation technique is used to solve the three-dimensional transonic small-disturbance equation for flow past a finite lifting wing. It is a development and extension of a technique presented by Murman and Cole[12] for two-dimensional problems and is similar to the method of Ballhaus and Bailey[21]. A second-order term in the perturbation potential, which represents a cross-coupling between derivatives in the wing plane, is included in the treatment. For simplicity the wing boundary conditions are satisfied on a plane. The numerical procedures are designed for the computation of fields with supersonic regions and shock waves embedded in a subsonic main stream, as well as flows with a sonic or supersonic stream containing embedded subsonic regions. The treatment of the wake takes account of the planar vortex sheet associated with a lifting

THIS DOCUMENT PROVIDED BY THE ABBOTT AEROSPACE
TECHNICAL LIBRARY
ABBOTTAEROSPACE.COM

wing and extending an infinite distance downstream. For flexibility, and economy of grid points, the co-ordinate system is chosen to be approximately swept with the wing. A concentration of grid points near the leading edge is obtained by an analytic stretching of a single transformed co-ordinate. Similar stretchings are used to control the distribution of points in the other two directions, and to reduce the half-space $y \geqslant 0$ to a finite computing region. Whatever the planform, the actual computation is performed on a uniform finite-difference grid.

Calculations by the TSP method have been made by Albone for the wing of Fig.1 (see also section 3) at one Mach number $M_\infty = 0.84$ and eleven incidences $\alpha = -1.93(0.40)2.07$ degrees. The grid points ($60 \times 24 \times 40$) included 35 chordwise and 18 spanwise stations ($y > 0$) within the planform, but the present analysis is confined to the single spanwise station $\eta = 0.750$. The pressure distributions on the upper and lower surfaces at $\alpha = -1.13$, -0.33, 0.47 and 1.27 degrees are shown on the upper diagrams of Figs.2 and 3. The gradients $-\partial C_{pu}/\partial\alpha$ and $+\partial C_{p\ell}/\partial\alpha$ (rad^{-1}) have been calculated from quartic polynomial fits to the data points at incidences α_0, $\alpha_0 \pm 0.4$ and $\alpha_0 \pm 0.8$ degrees. The values are plotted in the lower diagrams of Figs.2 and 3 and are listed in Table 1 together with the linear result $\frac{1}{2}\partial\ell/\partial\alpha$ from Ref.3. The latter is calculated by means of interpolation between solutions for $M_\infty = 0.60$, 0.80 and 0.86, each with four chordwise terms ($N = 4$), 23 spanwise terms and 95 spanwise integration stations between the wing tips.

Supercritical effects on the lower surface are apparent in the curve of $\partial C_{p\ell}/\partial\alpha$ at $\alpha_0 = -1.13$ degrees, mainly close to the leading edge but also just ahead of mid-chord. The next incidence $\alpha_0 = -0.33$ degrees has relatively mild supercritical flow, as the minimum $C_{p0} = -0.584$ corresponds to a local Mach number $M_0 = 1.135$; the distributions of $-\partial C_{pu}/\partial\alpha$ and $+\partial C_{p\ell}/\partial\alpha$ are at their closest to each other, but are significantly different from the curve of the linearized quantity $\frac{1}{2}\partial\ell/\partial\alpha$ added to Fig.2. At the higher incidences in Fig.3 there are two marked peaks and troughs in $-\partial C_{pu}/\partial\alpha$. While the leading-edge peak still dominates at $\alpha_0 = 0.47$ degrees, the peak at mid-chord is the salient feature at $\alpha_0 = 1.27$ degrees. In both cases a large influence on the oscillatory pressures can be anticipated. Any difficulties associated with very large local values of $\partial C_p/\partial\alpha$ near a strong shock wave could be overcome on the basis of equation (48) derived in section 5.1

THIS DOCUMENT PROVIDED BY THE ABBOTT AEROSPACE
TECHNICAL LIBRARY
ABBOTTAEROSPACE.COM

4.2 Oscillatory calculations

To carry out the calculations at one streamwise section of the wing for a given subsonic stream Mach number M_∞, frequency parameter $\bar{\nu}$ and mode of oscillation, the following information is required:

coefficients Γ_q/α ($q = 1$ to N) for steady flow at uniform incidence,

complex coefficients $\bar{\Gamma}_q$ ($q = 1$ to N) for the mode of oscillation,

aspect ratio $A = 2s/\bar{c}$, local leading edge $x_L/\bar{c}$ and chord $c/\bar{c}$,

set of values of ξ as determined by the grid of Ref.15,

corresponding sets of C_{pu0}, $C_{p\ell 0}$, $\partial C_{pu}/\partial\alpha$ and $\partial C_{p\ell}/\partial\alpha$ for each mean flow condition.

For simplicity, as in equation (30), the amplitude of oscillation is taken to be α_1. Then the sequence of calculations for equation (26) is as follows:

(a) $\partial\ell/\partial\alpha$ from equations (17) and (18) ($\omega = 0$, Γ_q for $\bar{\Gamma}_q$),

(b) $\bar{\ell}/\alpha_1$ from equations (17) and (18) ($\omega x/U_\infty = \bar{\nu}x/\bar{c}$),

(c) $\bar{K}/\alpha_1$ from equations (21) and (22), given $\bar{\ell}/\alpha_1$,

(d) $\dfrac{\bar{K}}{\alpha_1}\dfrac{(\partial C_p/\partial\alpha)_0}{\partial\ell/\partial\alpha} = \bar{J}$, say, see equations (26) and (32),

(e) integrand $\bar{H} = \bar{J}(U_\infty/U_0)/G$ involving equations (13) and (29) with $\gamma = 1.4$,

(f) $\bar{C}_p/\alpha_1$ from equation (26) which becomes

$$\frac{\bar{C}_p(\xi)}{\alpha_1} = \bar{J} + \frac{i\bar{\nu}cG}{\bar{c}}\int_0^\xi \bar{H}(\xi')d\xi' \quad . \tag{33}$$

The integration is conveniently carried out by the method of overlapping parabolas, in which each interval in ξ' contributes the average of the two results when the end points with alternatively the next fore or aft point are used to define the parabola.

When the simpler equation (28) is used instead of equation (26), steps (a), (b) and (c) lead to the final calculation in the form

THIS DOCUMENT PROVIDED BY THE ABBOTT AEROSPACE
TECHNICAL LIBRARY
ABBOTTAEROSPACE.COM

$$\frac{\bar{C}_p(\xi)}{\alpha_1} = \frac{(\partial C_p/\partial\alpha)_0}{\partial\ell/\partial\alpha}\left[\frac{\bar{K}}{\alpha_1} + \frac{U_\infty}{U_0}\left(\frac{\bar{\ell}}{\alpha_1} - \frac{\bar{K}}{\alpha_1}\right)\right] , \tag{34}$$

where U_∞/U_0 is given as a function of M_∞ and C_{p0} in equation (29). After $\bar{C}_p(\xi)/\alpha_1$ has been evaluated for each surface, the oscillatory chordwise loading of equation (31) is either evaluated as

$$\frac{\Delta\bar{C}_p}{\alpha_1} = \frac{\Delta C'_p}{\alpha_1} + i\bar{\nu}\left(\frac{\Delta C''_p}{\alpha_1\bar{\nu}}\right) \tag{35}$$

or in terms of its amplitude and phase

$$\frac{|\Delta\bar{C}_p|}{\alpha_1} = \left[\left(\frac{\Delta C'_p}{\alpha_1}\right)^2 + \left(\frac{\Delta C''_p}{\alpha_1}\right)^2\right]^{\frac{1}{2}} \tag{36}$$

and

$$\varepsilon_\Delta = \tan^{-1}\left(\Delta C''_p/\Delta C'_p\right) . \tag{37}$$

The present illustrative calculations are for the model of Fig.1 in rigid oscillation about the given swept axis at a frequency of 120 Hz, which for $M_\infty = 0.84$ corresponds to the frequency parameter $\bar{\nu} = 0.393$. The wing geometry gives $A = 7.425$, and at $\eta = 0.750$ we have $x_L/\bar{c} = 1.632$ and $c/\bar{c} = 0.725$. The coefficients in the linearized chordwise loading are calculated by interpolation in η and M_∞ between solutions for $M_\infty = 0.60$, 0.80 and 0.86 in steady flow or with the given frequency of 120 Hz; from the method of Ref.3 with 4 chordwise terms, 23 spanwise terms and 95 spanwise integration stations between the wing tips, the following values are obtained at $\eta = 0.750$.

q	$\bar{\nu} = 0$ Γ_q/α	$\bar{\nu} = 0.393$ $\bar{\Gamma}_q/\alpha_1$
1	0.3588	0.2424 + i0.1291
2	0.0179	0.0730 - i0.0909
3	-0.0054	-0.0167 - i0.0113
4	0.0000	-0.0011 + i0.0022

THIS DOCUMENT PROVIDED BY THE ABBOTT AEROSPACE
TECHNICAL LIBRARY
ABBOTTAEROSPACE.COM

The 35 values of ξ are given in Table 1, together with $\partial C_{pu}/\partial\alpha$ and $\partial C_{p\ell}/\partial\alpha$ for four mean-flow conditions, while the corresponding distributions of C_{pu0} and $C_{p\ell0}$ are plotted in Figs.2 and 3.

The results in Tables 2a and 2b for selected values of ξ are given in terms of amplitude and phase, as defined in equations (36) and (37); they cover linearized theory, equation (26) for each of the mean incidences $\alpha_0 = -1.13(0.8)1.27$ degrees and equation (28) for the most interesting of these cases $\alpha_0 = 1.27$ degrees. From these tables in conjunction with Fig.4, $|\Delta\bar{C}_p|/\alpha_1$ (rad^{-1}) is seen to be markedly different from the linearized curve in the range $0.05 < \xi < 0.45$, whatever the value of α_0; while there is an effect of frequency parameter, the broad pattern of behaviour is consistent with that of $(\partial C_{p\ell}/\partial\alpha - \partial C_{pu}/\partial\alpha)$, which has already been discussed in section 4.1 with reference to Figs.2 and 3. According to linearized theory ε_Δ is almost linear in ξ; relative to the wing motion the oscillatory loading shows a phase lag for $\xi < 0.4$ and a phase lead for $\xi > 0.4$. As calculated from equation (26), the influence of transonic flow is to delay the change-over from phase lag to phase lead and to increase the phase lead downstream of about mid-chord. The curve of ε_Δ for $\alpha_0 = -0.33$ degrees is omitted from Fig.4, as it is practically indistinguishable from that for $\alpha_0 = -1.13$ degrees. At the higher mean incidences the region of greatest importance lies near the downstream end of the embedded supersonic flow. As $|\Delta\bar{C}_p|/\alpha_1$ falls from its peak value in this region, ε_Δ increases rapidly to give a phase lead in excess of a quarter cycle: it should also be noted that the amplitude of oscillatory pressure fails to reach zero at the trailing edge. Both phenomena will be discussed later in relation to equation (28) and the experimental behaviour of ε_Δ.

It is instructive to consider the real and imaginary parts of the oscillatory surface pressure coefficients

$$\left.\begin{aligned} -\bar{C}_{pu} &= -C'_{pu} - iC''_{pu} \\ \bar{C}_{p\ell} &= C'_{p\ell} + iC''_{p\ell} \end{aligned}\right\}, \qquad (38)$$

both of which tend to

$$\tfrac{1}{2}\bar{\ell} = \tfrac{1}{2}\ell' + \tfrac{1}{2}i\ell'' \qquad (39)$$

THIS DOCUMENT PROVIDED BY THE ABBOTT AEROSPACE
TECHNICAL LIBRARY
ABBOTTAEROSPACE.COM

from equation (17) in the special case of linearized theory. With appropriate weighting factors these may be regarded as elementary contributions to the in-phase and in-quadrature aerodynamic forces required in flutter calculations. In three dimensions to first order in frequency the in-quadrature component is proportional to $\bar{\nu}$, and it is useful to present graphs of $-C'_{pu}/\alpha_1$, $+C'_{p\ell}/\alpha_1$, $-C''_{pu}/\alpha_1\bar{\nu}$ and $+C''_{p\ell}/\alpha_1\bar{\nu}$ in Figs.5 and 6. For $\alpha_0 = -1.13$ degrees there are two peaks in local supersonic Mach number on the lower surface; corresponding to $-C_{p\ell 0}$ in Fig.2, the forward peak reaches $M_0 = 1.3$ and gives rise to $C'_{p\ell}/\alpha_1 = 40$ and $C''_{p\ell}/\alpha_1\bar{\nu} = -60$, while the other at $\xi = 0.4$ reaches $M_0 = 1.15$ and causes relatively small fluctuations of approximately ±2 in the oscillatory components as plotted in Fig.5. At $\alpha_0 = -0.33$ degrees, when the supercritical effects are small, the upper and lower surfaces make similar contributions to the oscillatory loading, which are seen in Fig.5 to differ appreciably from that based on linearized theory and equation (39). With reference to Figs.3 and 6 at the higher values of α_0 the interest lies in the upper surface. At $\alpha_0 = 0.47$ degrees the forward peak ($M_0 = 1.325$ at $\xi = 0.04$) gives local peaks in $-C'_{pu}/\alpha_1$ and $C''_{pu}/\alpha_1\bar{\nu}$ of about 1.8 times the local value from linearized theory, while the recompression from $M_0 = 1.20$ to 1.05 near $\xi = 0.4$ causes peak-to-peak changes of 21 and 17 in $-C'_{pu}/\alpha_1$ and $-C''_{pu}/\alpha_1\bar{\nu}$ respectively, which could be important. These effects are intensified at $\alpha_0 = 1.27$ degrees; the forward peak ($M_0 = 1.50$ at $\xi = 0.04$) gives local peaks in $-C'_{pu}/\alpha_1$ and $C''_{pu}/\alpha_1\bar{\nu}$ of about 2.5 times the local value from linearized theory, while the recompression from $M_0 = 1.315$ to 1.00 near $\xi = 0.5$ causes peak-to-peak changes as high as 38 and 25 in $-C'_{pu}/\alpha_1$ and $-C''_{pu}/\alpha_1\bar{\nu}$ respectively. It would be surprising if changes of this magnitude did not involve major corrections to the generalized aerodynamic forces as predicted by linearized theory, and hence to significant changes in the flutter boundaries in the lower transonic speed range.

The chordwise distributions of $\Delta C''_p/\alpha_1\bar{\nu}$ for $\alpha_0 = 1.27$ degrees in Fig.7 illustrate crucial differences between calculations by the various theoretical methods. The inadequacy of linearized theory, especially near the leading edge and both during and after the recompression, is not in doubt. But it is well to question the relative status of equations (26) and (28). Both methods of calculation involve the two basic assumptions of equations (15) and (23). It may be wondered how well equation (15) holds near the trailing edge in view of the cross flow and whether it is impaired by viscous effects; moreover, difficulty might be anticipated in matching the velocity potentials from the upper and lower surfaces, as the mean flows from points immediately above and below the dividing streamline near the leading edge would have diverged laterally at the trailing

THIS DOCUMENT PROVIDED BY THE ABBOTT AEROSPACE
TECHNICAL LIBRARY
ABBOTTAEROSPACE.COM

edge. Perhaps $\partial\bar{\Phi}/\partial x$ should be replaced by the derivative of $\bar{\Phi}$ in the local flow direction. The consequences of any deficiencies in the treatment of Bernoulli's equation are not easily determined, but the failure of equation (26) to give zero oscillatory loading at the trailing edge is tentatively attributed to this approximation. It may also be wondered whether equation (23) deteriorates with increase in frequency parameter, but only rigorous numerical solutions of the equations of unsteady transonic flow are likely to settle the theoretical question. The further assumption in replacing equation (26) by equation (27) would not be expected to have much influence on the results near the leading edge, but elsewhere its only merits are the relative simplicity of the result in equation (28) and the re-establishment of the condition of zero oscillatory loading at the trailing edge. It will be seen in sections 5.2 and 6 that these possible advantages are offset by less favourable comparisons with experiment.

5 SEMI-EMPIRICAL METHOD

The preliminary investigation of Ref.1 has already shown the feasibility of a semi-empirical approach to the urgent problem of oscillatory aerodynamic loading in mixed subsonic and supersonic flow. The approximate theory of section 3, even in the integral form of equation (26) or (33), remains simple enough to lend itself to semi-empirical treatment.

Although the calculations depend on the chordwise distributions of both C_{p0} and $(\partial C_p/\partial\alpha)_0$, they are more sensitive to the latter. From theoretical considerations $(\partial C_p/\partial\alpha)_0$ becomes increasingly non-linear as the supercritical flow develops with increasing M_∞, or with increasing α_0 as shown in Fig.3. Meanwhile experimental evidence points to increasingly large viscous losses under supercritical conditions, so that the dependence of $(\partial C_p/\partial\alpha)_0$ on Reynolds number becomes of major importance. Thus we should not expect good quantitative agreement between the calculations of section 4.2 and the dynamic measurements of Ref.2. If, however, both C_{p0} and $(\partial C_p/\partial\alpha)_0$ are deduced from the corresponding static measurements, equation (26) becomes semi-empirical in the sense in which the simpler and more approximate equation (28) was treated in Ref.1. Moreover, as explained in section 5.1, there is also the possibility to allow for the effect of amplitude α_1. The calculations of section 5.2 therefore stand a greater chance of predicting the dynamic measurements at the particular Reynolds number.

THIS DOCUMENT PROVIDED BY THE ABBOTT AEROSPACE
TECHNICAL LIBRARY
ABBOTTAEROSPACE.COM

With practical application in mind, it is worth noting that detailed static experimental data over a range of incidence will normally be available at the stage of aircraft design when the problem of flutter clearance has to be faced.

5.1 Use of static experimental data

In the dynamic experiments of Ref.2 the half-model has fairly low flexibility, so that in the present calculations it may be assumed to oscillate rigidly about the swept axis $x = x_a$ as defined in Fig.1. Since

$$x_a/\bar{c} = 0.709 + (s/\bar{c})|\eta| \tan 25^o \quad , \tag{40}$$

the mode of oscillation corresponds to an upward vertical displacement

$$\begin{aligned} z/\bar{c} &= (\alpha - \alpha_0)(x_a - x)/\bar{c} \\ &= [0.709 + 1.731|\eta| - (x/\bar{c})]\, \Re\left\{\alpha_1 e^{i\omega t}\right\} \quad . \end{aligned} \tag{41}$$

Under quasi-steady conditions the oscillatory lift coefficient is simply

$$C_p = C_p(\alpha) \qquad \text{with} \qquad \alpha = \alpha_0 + \Re\left\{\alpha_1 e^{i\psi}\right\} \qquad \text{and} \qquad \psi = \omega t \quad . \tag{42}$$

When $C_p(\alpha)$ is non-linear, we write

$$C_p = C_{p0} + \sum_{r=1}^{R} A_r \cos r\psi \tag{43}$$

which for fixed values of α_0 and α_1 is a polynomial in

$$\alpha = \alpha_0 + \alpha_1 \cos \psi \quad . \tag{44}$$

The usual Fourier analysis gives

$$A_r = \frac{1}{\pi} \int_0^{2\pi} C_p(\alpha) \cos r\psi d\psi \quad . \tag{45}$$

With neglect of higher harmonics $r \geqslant 2$, equations (10) and (43) become consistent if

$$(\bar{C}_p)_{\bar{\nu}=0} = A_1 = \frac{1}{\pi} \int_0^{2\pi} C_p(\alpha) \cos \psi d\psi \quad . \tag{46}$$

THIS DOCUMENT PROVIDED BY THE ABBOTT AEROSPACE
TECHNICAL LIBRARY
ABBOTTAEROSPACE.COM

Equation (32) is then re-written as

$$\left(\frac{\bar{C}_p}{\bar{\ell}}\right)_{\bar{v}=0} = \frac{(\partial C_p/\partial\alpha)_1}{\partial\ell/\partial\alpha} \qquad (47)$$

where

$$(\partial C_p/\partial\alpha)_1 = \frac{1}{\pi\alpha_1}\int_0^{2\pi} C_p(\alpha)\cos\psi d\psi \qquad (48)$$

is a function of both α_0 and α_1 with the limiting value $(\partial C_p/\partial\alpha)_0$ as α_1 tends to zero. Equation (48) is clearly applicable whether $C_p(\alpha)$ is obtained from a theoretical or an experimental source.

The experimental determination of $(\partial C_p/\partial\alpha)_1$ is crucial to the semi-empirical method and may require data at closer intervals in α than usual. When Ref.1 was issued the coverage in α was unusually sparse, and there was no practical alternative to taking $(\partial C_p/\partial\alpha)_0$ as the linear slope between two values of α, one of which was outside the range of oscillation. However, Ref.2 includes more recent static data for $\alpha = 1.57(0.1\dot{6})2.57$ degrees, which make it possible to examine the dependence of equation (48) on α_0 and α_1.

The behaviour of $C_p(\alpha)$ at positions close to a shock wave is difficult to define on the basis of a few experimental points. The intermediate variation is not necessarily well represented by a polynomial through all the data points. The desirability of a discontinuous representation is arguable, but in any case this would require a closer spacing in both α and ξ to achieve adequate definition in the present application. A crude, but relatively safe, procedure would be to use segmented lines between consecutive data points. The preferred treatment is to apply the principle of least squares to obtain the best sinusoidal fit to C_p regarded as a function of ψ, for which purpose it is important to have experimental data at $\alpha = \alpha_0 \pm \alpha_1$; this procedure is equivalent to fitting a linear function $C_p(\alpha)$ to the data in the range $|\alpha - \alpha_0| \leqslant \alpha_1$. For five equally spaced values of α

$$(\partial C_p/\partial\alpha)_1 = \frac{1}{5\alpha_1}\Big[-2C_p(\alpha_0 - \alpha_1) - C_p(\alpha_0 - \tfrac{1}{2}\alpha_1) + C_p(\alpha_0 + \tfrac{1}{2}\alpha_1) + 2C_p(\alpha_0 + \alpha_1)\Big] . \qquad (49)$$

THIS DOCUMENT PROVIDED BY THE ABBOTT AEROSPACE
TECHNICAL LIBRARY
ABBOTTAEROSPACE.COM

Similarly with seven data points

$$(\partial C_p/\partial\alpha)_1 = \frac{3}{28\alpha_1}\left[-3C_p(\alpha_0 - \alpha_1) - 2C_p\left(\alpha_0 - \frac{2}{3}\alpha_1\right) - C_p\left(\alpha_0 - \frac{1}{3}\alpha_1\right) + C_p\left(\alpha_0 + \frac{1}{3}\alpha_1\right) + 2C_p\left(\alpha_0 + \frac{2}{3}\alpha_1\right) + 3C_p(\alpha_0 + \alpha_1)\right] . \quad (50)$$

It has been verified in practice that equation (50) gives results reasonably close to those obtained with segmented lines and with the best cubic fit to $C_p(\alpha)$.

Numerical results with the aid of equations (49) and (50) are illustrated in Tables 3 and 4. For α_0 = 2.07 degrees and α_1 = 0.$\dot{3}$ degrees = 0.0058 radians, the values of $-C_{pu0}$, $-C_{p\ell 0}$, $-(\partial C_{pu}/\partial\alpha)_1$ and $+(\partial C_{p\ell}/\partial\alpha)_1$ for the section η = 0.535 at stream Mach numbers from 0.80 to 0.86 are listed in Table 3. For η = 0.766 and M_∞ = 0.84 in Table 4, the corresponding quantities are shown for three values of α_0 and the influence of α_1 on the gradients is examined. Apart from the negative values of $(\partial C_{p\ell}/\partial\alpha)_1$ at ξ = 0.612 , which are not regarded as spurious experimental data, the rates of change of pressure on each surface from transonic small perturbation theory at α_0 = 1.27 degrees in Table 1 and from experiment at α_0 = 2.24 degrees in Table 4 show a strong qualitative resemblance. The smaller experimental peak values reflect the influence of the boundary layers, and perhaps also the smoothing process implicit in the use of least squares in equation (49). But, as in section 6, such quantitative comparisons are better made at given mean lift. The data in Tables 3 and 4 are thought to embody the essence of non-linearity in the real flow.

5.2 Comparisons with dynamic measurements

The experimental counterpart to the present theoretical investigation is reported in Ref.2. Most of the dynamic measurements on the half-wing model of Fig.1 in harmonic oscillation about the swept axis have been made for the mean incidence α_0 = 2.07 degrees and at the frequency of 120 Hz used throughout the theoretical calculations. There are, however, a few measurements for α_0 = -1.28 degrees, when supercritical flow occurs first on the lower surface. The unsteady pressures have been recorded from individual transducers at 50 positions on the planform at the five streamwise sections indicated in Fig.1, of which we shall be concerned with the outer three. The experimental range

THIS DOCUMENT PROVIDED BY THE ABBOTT AEROSPACE
TECHNICAL LIBRARY
ABBOTTAEROSPACE.COM

of Mach number $0.60 \leqslant M_\infty \leqslant 0.86$ is fully covered in the calculations. As described in the preliminary presentation of Ref.1, the measurements have revealed some dramatic changes in the distribution of oscillatory surface pressure as the transonic flow develops.

Equations (31) and (33) are used to calculate the oscillatory wing loading by the procedure described in the paragraph of section 4.2 containing the latter equation. In contrast to the purely theoretical calculations of section 4.2, however, the static data are now taken from experiment in accord with section 5.1 The semi-empirical calculations are confined to the three sections $\eta = 0.535$, 0.766 and 0.882, because these show the largest response to supercritical flow and are free from any peculiarities associated with the trailing-edge crank and the reflection plane at the tunnel wall. The section $\eta = 0.535$ is considered systematically over the whole range of Mach number. The combination $\eta = 0.766$ and $M_\infty = 0.84$ is selected in order to study the influence of mean incidence and amplitude of oscillation. The results are presented together with experimental values in Tables 5 to 7 and in Figs.8 to 17, usually as the real and imaginary parts or the amplitude and phase angle of the wing loading $\Delta\bar{C}_p$ in equations (35) to (37), but in one instance as the real and imaginary parts of $\bar{C}_p$ on the individual surfaces.

Table 5 shows listings of the semi-empirical and measured values of amplitude $|\Delta\bar{C}_p|/\alpha_1$ and phase ε_Δ at the three sections for $M_\infty = 0.86$. Similar characteristics are found at each section. Both calculation and experiment indicate peaks in amplitude near the leading edge and also in the region $0.3 \leqslant \xi \leqslant 0.5$; they give a consistent phase lag of about 30 degrees near the leading edge changing to large phase leads somewhere in the region $0.60 < \xi < 0.85$. In finer detail the discrepancies between the semi-empirical and measured amplitudes do not show such a consistent pattern; the magnitudes of the second peaks in $|\Delta\bar{C}_p|/\alpha_1$ appear to be overestimated at $\eta = 0.535$, underestimated at $\eta = 0.766$ and in good agreement at $\eta = 0.882$. While the changes in the sign of ε_Δ are satisfactorily predicted near mid-chord in each case, the measured phase lags just forward of this and phase leads when $\xi \geqslant 0.7$ are underestimated by the semi-empirical method.

Static data from Table 3 for $\eta = 0.535$ are used in obtaining the semi-empirical results for supercritical flow in Table 6. Here the oscillatory wing loading near the leading edge is in good agreement with the measurements at each of the four Mach numbers. Moreover, the peak amplitude and its rearward movement

THIS DOCUMENT PROVIDED BY THE ABBOTT AEROSPACE
TECHNICAL LIBRARY
ABBOTTAEROSPACE.COM

with increasing Mach number are well predicted. Likewise the change in sign of ε_Δ is correctly predicted to move rearwards as M_∞ increases. The tendency to underestimate the phase lag just forward of the change-over is more pronounced than in Table 5, while the underestimate of the phase lead is less marked when $\xi \geqslant 0.7$.

The real and imaginary parts of $\Delta\bar{C}_p$ for $\eta = 0.766$ are presented for four supercritical Mach numbers in Table 7. The rearward movements in the peak value of $\Delta C_p'/\alpha_1$ and the zero value of $\Delta C_p''/\alpha_1\bar{\nu}$ with increasing M_∞ now become the main features of both calculation and experiment; the increment of 0.06 from $M_\infty = 0.80$ to 0.86 produces shifts of roughly 0.3 chord. However, while the measurements indicate that the strength of the in-phase peak in $\Delta C_p'/\alpha_1$ is maintained up to $M_\infty = 0.86$, the calculations at this highest Mach number fail to reproduce this characteristic. Moreover, although the in-quadrature peak in $-\Delta C_p''/\alpha_1\bar{\nu}$ is reasonably well predicted at $M_\infty = 0.80$, the calculations at higher M_∞ become progressively less successful as the location of the peak moves rearward. Yet, judged against the performance of linear theory, the semi-empirical method will be seen to have achieved a good deal.

The first of the graphical presentations, Fig.8, shows the serious inadequacy of linear theory when $M_\infty = 0.84$. Its main purpose is to illustrate at $\eta = 0.535$ the significant improvement in the present calculations through the use of more detailed static experimental data, denoted by Ref.2, in place of the limited information available when Ref.1 was written. Fig.8 also demonstrates the quite small effect on $\Delta C_p'/\alpha_1$ in changing from the old formula in equation (28), as used in Ref.1, to the preferred equation (26). The merit of the latter equation is illustrated in Fig.9 by the predicted distributions of $\Delta C_p''/\alpha_1\bar{\nu}$ over the rear half of the chord. Equation (26) provides values greater than those from linear theory in place of the much smaller values from equation (28). Although the predictions in this region remain typically below the experimental results, the improvement is worth the small cost in computational effort. The next example in Fig.10 shows the real and imaginary parts of the distributions of oscillatory pressure coefficient $\bar{C}_p$ on the upper and lower surfaces of the wing at $\eta = 0.766$ when $M_\infty = 0.82$. The relatively small departure from linear theory featured in the measured lower-surface pressures is reproduced by the semi-empirical method; however, the peculiar abnormality near $\xi = 0.6$ already noted in the static data of Table 4 at $M_\infty = 0.84$ is also present at this lower Mach number in the local behaviour

THIS DOCUMENT PROVIDED BY THE ABBOTT AEROSPACE
TECHNICAL LIBRARY
ABBOTTAEROSPACE.COM

of $C'_{p\ell}$ and $C''_{p\ell}$ from dynamic measurement and calculation alike. The semi-empirical in-phase and in-quadrature components on the upper surface both indicate an encouraging measure of success.

Figs.11 and 12 compare the linear theoretical results from $\eta = 0.766$ and $M_\infty = 0.84$ with the experimental and semi-empirical ones at two different mean incidences. The lower incidence $\alpha_0 = -1.28$ degrees is a case of small negative lift when the supercritical flow is primarily on the lower surface. The rates of change $\partial C_p/\partial\alpha$ are deduced from steady measurements at -1.28 and -0.28 degrees, so that the semi-empirical curves in Fig.11 may suffer through lack of closely spaced static data. The real part of $\Delta\bar{C}_p$ is reasonably well predicted, but the imaginary part is underestimated where $\xi \geqslant 0.4$. The other case in Fig.12 is one of the most striking examples from the oscillations about $\alpha_0 = 2.07$ degrees. The semi-empirical method is again fairly successful as regards $\Delta C'_p/\alpha_1$: the calculated chordwise behaviour of $\Delta C''_p/\alpha_1\bar{\nu}$ is too gentle, but the two peaks and the trough are correctly positioned. The extra quasi-steady curve of

$$\Delta C'_p/\alpha_1 = (\partial C_{p\ell}/\partial\alpha)_1 - (\partial C_{pu}/\partial\alpha)_1 \qquad (51)$$

represents the special case of zero frequency common to experiment and the semi-empirical method. Regarding the latter now as a theoretical means of correcting the measured static data for frequency parameter, we see that the effect is significant. The shape of the quasi-steady curve in Fig.12 is mirrored by both the semi-empirical method and the experiments, but again the peak in the experimental curve is much greater.

A further illustration of the calculated frequency effect is included for $\eta = 0.535$ and $M_\infty = 0.82$ in Fig.13. However, the main purpose of Figs.13 and 14 is to demonstrate the influence of Mach number on the oscillatory components of wing loading. By and large the discrepancies in $\Delta C'_p/\alpha_1$ between experiment and semi-empirical calculation do not appear to increase to a great extent as M_∞ grows from 0.60 to 0.84. The general tendency in Fig.13 is for the peak in-phase component to reach its maximum soon after the flow becomes supercritical; thereafter the peak becomes lower but of wider base. Negative values over the rear part are measured at $M_\infty = 0.80$ but are not predicted at this section until $M_\infty = 0.84$. The semi-empirical method still fails to provide the large increase in phase lag corresponding to the large negative experimental values of $\Delta C''_p/\alpha_1\bar{\nu}$ in the supercritical region. Although the calculations again

THIS DOCUMENT PROVIDED BY THE ABBOTT AEROSPACE
TECHNICAL LIBRARY
ABBOTTAEROSPACE.COM

show the correct trends away from linear theory in Fig.14, the displacements could be doubled with good effect throughout the range of Mach number, but without apparent theoretical justification. All the preceding comments apply to the additional results for $\eta = 0.535$ at $M_\infty = 0.86$ in Fig.15, which also includes a case of good agreement between both components of the measured and semi-empirical oscillatory loading for $\eta = 0.882$ at the same Mach number. This favourable result has already been discussed in relation to Table 5.

The final sets of curves by means of the semi-empirical method in Figs.16 and 17 demonstrate the calculated effects of changes in mean incidence and amplitude of oscillation in accord with the measured static data of Table 4. Both α_0 and α_1 have important influences on $|\Delta\bar{C}_p|/\alpha_1$, but these appear to be local in character. While the local dependence of $\Delta\bar{C}_p$ on α_1 can be highly non-linear, the semi-empirical curves for $\alpha_1 = 0.003$ and 0.009 radians in Fig.17 are only about as different from each other as from the dynamic measurements when $\alpha_1 = 0.006$ radians. Neither α_0 nor α_1 seems to have much effect on phase angle, but ε_Δ is always liable to be sensitive when $|\Delta\bar{C}_p|/\alpha_1$ is small. It stands to reason that the measurements themselves are likely to be non-linear in amplitude.

In general, we may conclude that the present comparisons are significantly better than those in Ref.1, on account of the removal of the approximation leading to equation (27) and through the careful analysis of more detailed static experimental data in section 5.1. The theoretical investigation has added confidence to the interpretation of the experimental results in Ref.2.

6 DISCUSSION

The method of calculation formulated in section 3 and applied in sections 4 and 5 is of considerable generality. It is at present limited to subsonic flow in the undisturbed stream and to wings in isolation, but the same principles could be applied to a supersonic stream or, for example, to a T-tail. The following table summarizes how the various parameters enter into the calculation, and we shall consider in turn the practical significance of each of them.

THIS DOCUMENT PROVIDED BY THE ABBOTT AEROSPACE
TECHNICAL LIBRARY
ABBOTTAEROSPACE.COM

Parameter	Non-linear static data	Linear theoretical data
Planform	Yes	Yes
Mach number	Yes	Yes
Frequency parameter	No	Yes
Mode of oscillation	No	Yes
Aerofoil section	Yes	No
Camber and twist	Yes	No
Mean incidence	Yes	No
Oscillatory amplitude	Yes	No
Reynolds number	If available	No

Planform and Mach number are basic to all aspects of the problem. The present investigation is confined to a single planform of practical interest for civil aircraft. There is need to examine a variety of shapes, and especially any cases where there is reason to probe the hazard of transonic flutter. The present results have shown how dramatically the oscillatory chordwise loadings can be expected to vary with small changes of Mach number in the supercritical range, and the message is amply reinforced by the experimental evidence. What is not yet appreciated is the extent to which the large chordwise fluctuations are neutralized in the generalized forces that influence the flutter characteristics. Another aspect that calls for investigation is that the dependence on Mach number may be subject to the philosophy of design. We contrast the transonic behaviour of a wing designed for supersonic operation with that in the high subsonic flight envelope of a wing specifically designed to cruise with supercritical surface flow. In either case it is uncertain how relevant the present results may prove to be, but it is easy to envisage dynamic problems of greater severity.

Frequency parameter and mode of oscillation may well influence the surface flow in respects beyond the scope of the present treatment. Although the frequency effect, represented by the difference between the quasi-steady and semi-empirical curves of $\Delta C_p'/\alpha_1$ in Figs.12 and 13, gives some reassurance, the tendency to underestimate the magnitude of $\Delta C_p''/\alpha_1\bar{\nu}$ during and after recompression on the suction surface suggests that the method may be capable of improvement by appealing to the non-linear differential equation of unsteady transonic flow. Nevertheless, the present formulation is quite general in frequency and, as this only occurs in the linear part of the analysis, the method

THIS DOCUMENT PROVIDED BY THE ABBOTT AEROSPACE
TECHNICAL LIBRARY
ABBOTTAEROSPACE.COM

can be regarded as applicable to the boundary condition of equation (41) with arbitrary time dependence and mode of oscillation. When the mode is changed it is debatable whether to adopt the simplification in equation (32), as discussed at the end of section 3.2. In particular, this question of an explicit link between the static data and the mode of oscillation will become crucial when the application to an oscillating control surface is considered, for this development is a matter of urgency.

The remaining geometrical parameters only feature in the procurement of the necessary steady pressure distributions. Aerofoil section, camber and twist are principal elements in wing design and influence the nature of the transonic flow to be perturbed, whether the source is theoretical[15] or experimental[2]. The same considerations apply to mean incidence, but the variation of this parameter has been studied in Figs.4 to 6 and is found to be almost as important as that of free-stream Mach number. The powerful effects as regards chordwise pressure distribution make one wonder whether in a flutter calculation it is necessary to consider aeroelastic camber changes in addition to deformations in bending and torsion. It is explained in section 5.1 and illustrated in Fig.17 how the amplitude of oscillation can be taken into account. The essential aerodynamics can be distorted in the semi-empirical method by handling the static data at too widely or too closely spaced angles of attack. From the same viewpoint there are dangers in attempting to draw conclusions from transonic experiments in which the amplitude of oscillation is not varied, for flutter could be a non-linear phenomenon. Still, the effect of increasing amplitude seems to be to smooth out the sharp peaks to some extent. If these sharp peaks lead to worse flutter characteristics under supercritical conditions, there is an inference that increased amplitude might be favourable. It would then be sufficient to accept an adequate margin of safety for small-amplitude oscillations.

Reynolds number must account for much of the difference between calculations by the semi-empirical and theoretical methods. Some idea of the importance of this parameter can perhaps be gleaned from their separate comparisons with experiment. It is well-known in two dimensions that the inviscid transonic small-perturbation theory can give half as much lift again as high-speed wind tunnel tests on an aerofoil, so important do the boundary layers become at supercritical Mach numbers. When the TSP calculations at $\eta = 0.750$ including Figs.2 and 3 and the measured steady pressures at $\eta = 0.766$ are integrated to give local lift, the following coefficients are obtained for $M_\infty = 0.84$.

THIS DOCUMENT PROVIDED BY THE ABBOTT AEROSPACE
TECHNICAL LIBRARY
ABBOTTAEROSPACE.COM

α (degrees)	-1.28	-1.13	-0.33	0.47	1.27	2.07
C_{LL} (TSP)		0.06	0.20	0.34	0.49	0.64
C_{LL} (Exp)	-0.05					0.36

The main deficiency in measured lift arises from the loss in rear loading, presumably due to viscous effects, and leads to an alarming correction factor 0.56 to reconcile the theoretical and experimental values at $\alpha = 2.07$ degrees; to put these into perspective, linear theory gives $C_{LL} = 0.50$ midway between them. In Fig.18 the theoretical distributions of mean static pressure have been interpolated in α_0 to correspond to the experimental mean lift coefficient $C_{LL0} = 0.36$; the TSP calculations of oscillatory loading for this mean condition are then shown together with the same experimental distributions of $|\Delta\bar{C}_p|/\alpha_1$ and ε_Δ as those used in Fig.17. While it is not surprising that in Fig.17 the semi-empirical method fares so much better in relation to the dynamic measurements, in Fig.18 the excessive theoretical amplitude of oscillatory loading forward of $\xi = 0.3$ is a strong indication of the important part that Reynolds number can play. Nevertheless, the TSP and wind-tunnel data would be expected to err in opposite directions from the desired true prediction for full-scale Reynolds number. In looking towards future clarification, there is little doubt that allowance for boundary layers in the TSP calculations will be of great importance. Perhaps the crucial issue is whether this can improve the accuracy of representation of both the strength and the location of the shock wave system.

The other salient feature of Fig.18 is the poor showing of ε_Δ from equation (28), which reinforces the evidence in Fig.9 to justify the use of equation (26) in the present investigation. However, as discussed towards the end of section 4.2, there is the disadvantage that, unlike equation (28), equation (26) can give a non-zero oscillatory load at the trailing edge. This effect appears to be fairly small in Fig.18, but is more conspicuous in the behaviour of the in-quadrature component $\Delta C''_p$; the numerical implications may grow in importance with increasing frequency parameter. While it seems reasonable to treat the matter as a local defect by fairing $|\Delta\bar{C}_p|$ from its value at, say, $\xi = 0.80$ to zero at $\xi = 1$, such an expedient would have to be reviewed in the light of further experience.

THIS DOCUMENT PROVIDED BY THE ABBOTT AEROSPACE
TECHNICAL LIBRARY
ABBOTTAEROSPACE.COM

The pursuit of other theoretical methods should be encouraged, notably on the lines of Refs.11 to 16 which have been reviewed briefly in section 2.2. The primary need is for a fuller appreciation of the physics of unsteady viscous transonic flow through Ref.2 and its successors. Is it too much to hope that such insight could lead to a re-modelling of equations (15) and (23), the corner-stones of the present study?

7 CONCLUSIONS

(1) Through combined theoretical and experimental study a two-pronged attack on the prediction of oscillatory wing loading has been launched. The present formulation in equation (26) invites the substitution of steady aerodynamic pressures and their gradients either from non-linear theory or from experiment, with particular application to mixed subsonic and supersonic flows.

(2) In either case the method can be applied to any planform and takes account of aerofoil section, camber and twist, mean incidence, subsonic stream Mach number, frequency parameter, mode and amplitude of oscillation. The semi-empirical version admits Reynolds number as an important additional parameter. Until viscous effects are incorporated in the transonic small-perturbation theory, they are likely to be exaggerated on the basis of wind-tunnel data obtained at Reynolds numbers well below full scale.

(3) Either version reproduces qualitatively the marked characteristics of unsteady supercritical flow found in the experiments on a particular wing. The semi-empirical method allows successfully for the quantitative effect of frequency on the in-phase wing loading, but it tends to underestimate the large chordwise variations in the component in quadrature with the wing oscillation.

(4) There is an obvious need for continuing work on the oscillatory transonic problem through alternative theoretical approaches and more detailed experimental studies. It is desirable to extend the present theoretical treatment to oscillating control surfaces. A further combined study for an advanced super-critical wing design would be of special interest.

(5) It remains to establish the significance of the present investigation in the context of flutter prediction and, in particular, the extent to which the large chordwise variations are neutralized in the integration process leading to the generalized forces involved in flutter calculations. It is recommended that studies along these lines, to compare the predictions of linear and non-linear transonic aerodynamics, should be undertaken in close collaboration with the aircraft industry.

THIS DOCUMENT PROVIDED BY THE ABBOTT AEROSPACE
TECHNICAL LIBRARY
ABBOTTAEROSPACE.COM

Table 1

RATES OF CHANGE OF PRESSURE PER RADIAN INCIDENCE FROM LINEAR THEORY[3] AND FROM TSP THEORY[15] FOR VARIOUS INCIDENCES ($M_\infty = 0.84$, $\eta = 0.750$)

ξ	$\frac{1}{2}\frac{\partial \ell}{\partial \alpha}$	Values of $-\partial C_{pu}/\partial\alpha$ for $\alpha_0 =$				Values of $+\partial C_{p\ell}/\partial\alpha$ for $\alpha_0 =$			
		-1.13°	-0.33°	0.47°	1.27°	-1.13°	-0.33°	0.47°	1.27°
0.0037	39.53	6.05	5.68	5.30	4.30	9.67	19.68	16.06	11.51
0.0109	23.05	9.27	8.56	6.97	5.59	32.86	26.71	20.48	14.25
0.0188	17.48	12.64	11.73	20.43	7.06	57.21	27.24	20.60	14.52
0.0283	14.18	14.75	18.08	25.54	18.61	50.71	23.41	18.40	13.55
0.0404	11.78	14.15	18.49	20.00	29.02	29.61	17.81	15.38	11.88
0.0569	9.83	11.86	13.95	17.61	24.37	14.81	13.65	12.40	9.96
0.0796	8.21	9.72	11.43	13.23	15.22	11.76	10.83	10.09	8.28
0.1086	6.90	8.60	10.00	10.55	9.55	10.93	9.09	8.58	7.14
0.1421	5.90	8.14	9.38	9.91	7.30	9.52	7.92	7.55	6.36
0.1771	5.16	7.75	9.42	10.49	6.77	8.36	7.06	6.82	5.81
0.2121	4.60	7.30	9.38	11.69	6.92	7.67	6.58	6.36	5.46
0.2464	4.15	6.89	8.88	13.18	7.29	7.32	6.54	6.24	5.33
0.2799	3.79	6.51	8.10	14.98	7.76	7.27	6.67	6.28	5.31
0.3125	3.49	6.17	7.06	17.06	8.31	7.48	6.68	6.40	5.33
0.3444	3.23	5.77	5.94	19.07	8.93	8.05	6.82	6.54	5.49
0.3758	2.99	5.36	5.08	20.50	9.72	9.06	7.13	6.51	5.43
0.4068	2.79	4.95	4.80	20.46	11.41	9.84	7.04	6.15	4.97
0.4375	2.60	4.49	4.84	15.84	17.48	8.69	6.05	5.15	4.41
0.4680	2.43	3.99	4.61	3.04	32.79	4.57	4.03	4.07	3.78
0.4984	2.27	3.56	3.97	-7.93	44.54	1.83	2.62	3.31	3.17
0.5288	2.11	3.26	3.21	-7.68	16.32	1.76	2.26	2.75	2.68
0.5591	1.97	2.86	2.60	-3.68	-8.99	1.60	1.95	2.38	2.35
0.5894	1.83	2.43	1.92	-1.55	-5.15	1.44	1.73	2.09	2.09
0.6198	1.70	2.08	1.52	-0.65	-3.35	1.27	1.50	1.84	1.84
0.6502	1.58	1.72	1.34	-0.40	-2.17	1.10	1.30	1.59	1.62
0.6807	1.46	1.38	1.04	-0.22	-1.42	0.96	1.13	1.39	1.43
0.7112	1.34	1.13	0.85	-0.13	-1.00	0.83	0.98	1.22	1.26
0.7420	1.23	0.95	0.71	-0.10	-0.75	0.72	0.85	1.06	1.10
0.7729	1.11	0.77	0.57	-0.10	-0.59	0.61	0.73	0.93	0.97
0.8042	1.00	0.60	0.44	-0.12	-0.50	0.52	0.65	0.82	0.86
0.8359	0.88	0.46	0.33	-0.14	-0.43	0.45	0.57	0.72	0.77
0.8683	0.76	0.35	0.24	-0.17	-0.40	0.38	0.48	0.63	0.69
0.9016	0.64	0.22	0.13	-0.21	-0.39	0.30	0.40	0.54	0.59
0.9360	0.49	0.10	0.03	-0.26	-0.40	0.23	0.31	0.45	0.51
0.9721	0.31	-0.07	-0.13	-0.35	-0.45	0.12	0.18	0.34	0.41

THIS DOCUMENT PROVIDED BY THE ABBOTT AEROSPACE
TECHNICAL LIBRARY
ABBOTTAEROSPACE.COM

Table 2

THEORETICAL AMPLITUDE AND PHASE OF OSCILLATORY LOADING AT VARIOUS INCIDENCES ($M_\infty = 0.84$, $\eta = 0.750$)

ξ	Linear theory	Equation (26) with static data from TSP theory				Eqn. (28)
		$\alpha_0 = -1.13^\circ$	$\alpha_0 = -0.33^\circ$	$\alpha_0 = 0.47^\circ$	$\alpha_0 = 1.27^\circ$	$\alpha_0 = 1.27^\circ$
(a) Amplitude $\lvert\Delta\bar{C}_p\rvert/\alpha_1$ (rad^{-1})						
0.0109	37.12	33.91	28.39	22.10	15.97	15.97
0.0283	22.81	52.64	33.36	35.33	25.86	25.87
0.0569	15.80	21.42	22.16	24.09	27.56	27.58
0.1086	11.08	15.65	15.29	15.32	13.37	13.39
0.1771	8.30	12.88	13.15	13.75	10.05	10.09
0.2464	6.72	11.25	12.25	15.38	10.04	10.13
0.3125	5.69	10.84	10.88	18.41	10.76	10.98
0.3758	4.95	11.35	9.64	20.98	11.84	12.24
0.4375	4.38	10.34	8.59	16.24	16.80	17.77
0.4680	4.12	6.92	6.91	5.98	27.68	29.79
0.4984	3.89	4.68	5.43	3.70	35.76	39.52
0.5288	3.68	4.43	4.64	3.83	14.45	16.08
0.5591	3.48	4.08	4.03	2.10	4.98	5.60
0.5894	3.28	3.70	3.45	2.21	2.84	2.57
0.6198	3.10	3.40	3.08	2.45	2.29	1.25
0.6807	2.74	2.88	2.64	2.50	2.28	0.13
0.7420	2.39	2.59	2.38	2.47	2.39	0.43
0.8042	2.03	2.39	2.21	2.44	2.44	0.46
0.8683	1.63	2.26	2.07	2.40	2.46	0.42
0.9360	1.12	2.19	1.99	2.41	2.51	0.24
(b) Phase angle ε_Δ in degrees						
0.0109	-30.4	-30.7	-30.7	-30.6	-30.6	- 30.3
0.0283	-29.2	-29.9	-29.8	-29.8	-29.8	- 29.3
0.0569	-27.2	-27.7	-28.1	-28.2	-28.4	- 27.6
0.1086	-23.4	-24.4	-24.8	-24.8	-24.6	- 24.0
0.1771	-18.4	-20.3	-20.9	-21.1	-20.3	- 19.4
0.2464	-13.2	-16.4	-17.2	-18.1	-17.0	- 14.9
0.3125	- 8.1	-13.0	-13.5	-15.7	-14.3	- 10.6
0.3758	- 3.1	-10.5	- 9.7	-13.3	-12.0	- 6.4
0.4375	+ 1.7	- 6.8	- 5.8	- 8.8	-11.0	- 2.5
0.4680	4.1	- 0.6	- 1.8	+ 5.0	-11.5	- 0.5
0.4984	6.6	+ 8.2	+ 3.4	132.9	-10.8	+ 2.9
0.5288	9.0	11.1	7.8	135.0	- 4.3	6.5
0.5591	11.4	14.8	12.6	92.7	141.3	-172.2
0.5894	13.8	19.1	18.6	56.7	117.9	-171.0
0.6198	16.2	23.5	24.0	47.0	95.5	-170.9
0.6807	21.0	33.8	33.6	48.7	68.2	+ 61.4
0.7420	25.7	42.5	42.3	52.7	63.2	34.9
0.8042	30.6	50.6	49.9	57.2	63.5	38.2
0.8683	35.6	56.5	56.0	60.9	64.8	43.7
0.9360	40.8	62.5	62.2	64.7	67.3	54.0

THIS DOCUMENT PROVIDED BY THE ABBOTT AEROSPACE
TECHNICAL LIBRARY
ABBOTTAEROSPACE.COM

Table 3

MEASURED PRESSURE COEFFICIENTS AND THEIR MEAN RATES OF CHANGE FOR VARIOUS MACH NUMBERS (η = 0.535, α_0 = 2.07°, α_1 = 0.0058 rad)

ξ	Values of $-C_{pu0}$ for M_∞ =				Values of $-C_{p\ell 0}$ for M_∞ =			
	0.80	0.82	0.84	0.86	0.80	0.82	0.84	0.86
0.027	0.702	0.668	0.620	0.547	−0.061	−0.049	−0.019	+0.013
0.054	0.923	0.888	0.837	0.781	−0.067	−0.063	−0.041	−0.015
0.105	0.889	0.921	0.894	0.844	+0.014	+0.027	+0.042	+0.066
0.156	0.794	0.904	0.923	0.885	0.055	0.067	0.084	0.107
0.207	0.640	0.833	0.899	0.876	0.107	0.119	0.134	0.159
0.308	0.539	0.595	0.815	0.872	0.232	0.250	0.271	0.307
0.410	0.493	0.494	0.541	0.803	0.269	0.287	0.309	0.345
0.511	0.386	0.393	0.385	0.489	0.188	0.200	0.219	0.248
0.610	0.313	0.319	0.306	0.279	0.044	0.054	0.055	0.070
0.713	0.181	0.183	0.178	0.153	−0.074	−0.072	−0.067	−0.059
0.824	0.054	0.053	0.051	0.040	−0.151	−0.151	−0.152	−0.145
0.859	0.017	0.020	0.019	0.009	−0.185	−0.191	−0.191	−0.179

ξ	Values of $-(\partial C_{pu}/\partial\alpha)_1$ for M_∞ =				Values of $+(\partial C_{p\ell}/\partial\alpha)_1$ for M_∞ =			
	0.80	0.82	0.84	0.86	0.80	0.82	0.84	0.86
0.027	11.61	10.66	8.33	7.92	10.46	8.35	8.52	10.07
0.054	4.54	3.26	1.94	3.67	7.26	5.70	5.76	7.37
0.105	15.93	9.97	3.47	5.29	6.13	4.34	4.65	6.47
0.156	20.75	18.47	7.76	6.00	5.62	3.71	3.83	5.89
0.207	20.63	19.80	11.23	7.41	5.21	3.54	3.37	5.67
0.308	1.82	14.81	17.94	8.72	4.26	3.06	3.68	5.96
0.410	0.90	−1.46	10.16	14.70	3.87	2.41	2.89	5.28
0.511	0.03	−0.97	−1.65	5.31	3.41	2.11	2.20	3.82
0.610	0.43	+0.07	−1.96	2.50	2.02	0.68	0.58	2.19
0.713	0.50	−0.27	−1.09	1.35	2.29	0.64	0.43	1.98
0.824	0.07	−0.37	−0.53	1.00	1.28	0.25	−0.16	1.05
0.859	−0.42	+0.30	−0.03	1.92	2.32	0.71	0.44	1.72

THIS DOCUMENT PROVIDED BY THE ABBOTT AEROSPACE
TECHNICAL LIBRARY
ABBOTTAEROSPACE.COM

Table 4

MEASURED PRESSURE COEFFICIENTS AND THEIR MEAN RATES OF CHANGE FOR VARIOUS INCIDENCES AND AMPLITUDES ($M_\infty = 0.84$, $\eta = 0.766$)

				$\alpha_1 = 0.0058$ rad			$\alpha_0 = 2.07^\circ$		
ξ	$-C_{pu0}$ for $\alpha_0 =$			$-(\partial C_{pu}/\partial\alpha)_1$ for $\alpha_0 =$			$-(\partial C_{pu}/\partial\alpha)_1$ for $\alpha_1 =$		
	1.90°	2.07°	2.24°	1.90°	2.07°	2.24°	0.0029	0.0058	0.0087
0.024	0.328	0.355	0.361	7.18	6.18	10.18	5.69	6.18	8.93
0.107	0.911	0.935	0.935	6.29	4.56	4.88	4.09	4.56	5.70
0.157	0.924	0.944	0.949	6.08	5.80	5.02	4.37	5.80	5.79
0.208	0.926	0.935	0.961	9.52	8.82	7.29	6.03	8.82	8.81
0.310	0.856	0.860	0.920	25.40	17.37	11.69	11.04	17.37	19.63
0.411	0.478	0.494	0.637	14.64	16.48	20.56	27.21	16.48	15.95
0.512	0.325	0.321	0.318	-2.20	-1.42	1.68	-1.24	-1.42	-0.21
0.612	0.265	0.258	0.254	-3.51	-4.07	-1.82	-2.03	-4.07	-2.96
0.714	0.144	0.147	0.129	-1.55	-2.33	-2.34	-2.56	-2.33	-1.86
0.808	0.033	0.029	0.020	-1.03	-1.08	-1.07	-2.22	-1.08	-0.87
0.858	0.004	0.006	-0.004	-0.28	-0.72	-0.89	-1.38	-0.72	-0.49

				$\alpha_1 = 0.0058$ rad			$\alpha_0 = 2.07^\circ$		
ξ	$-C_{p\ell 0}$ for $\alpha_0 =$			$+(\partial C_{p\ell}/\partial\alpha)_1$ for $\alpha_0 =$			$+(\partial C_{p\ell}/\partial\alpha)_1$ for $\alpha_1 =$		
	1.90°	2.07°	2.24°	1.90°	2.07°	2.24°	0.0029	0.0058	0.0087
0.024	-0.063	-0.098	-0.114	8.84	8.22	6.98	8.82	8.22	7.80
0.107	+0.051	+0.034	+0.022	5.26	4.61	4.37	4.98	4.61	4.76
0.157	0.074	0.062	0.049	3.57	3.95	3.95	4.30	3.95	3.70
0.208	0.118	0.103	0.097	3.23	3.36	3.37	3.64	3.36	3.25
0.310	0.253	0.242	0.233	2.85	3.28	3.13	3.45	3.28	2.95
0.411	0.333	0.317	0.310	3.51	3.77	2.37	3.92	3.77	2.85
0.512	0.259	0.245	0.242	2.34	3.19	2.23	3.01	3.19	2.26
0.612	0.080	0.110	0.122	-5.95	-6.03	-3.82	-7.31	-6.03	-4.60
0.714	-0.057	-0.063	-0.069	+0.89	+0.83	+0.96	+1.93	+0.83	+0.74
0.808	-0.161	-0.164	-0.160	0.52	0.45	0.21	-0.14	0.45	0.45
0.858	-0.165	-0.170	-0.166	0.76	0.76	0.17	+0.21	0.76	0.54

THIS DOCUMENT PROVIDED BY THE ABBOTT AEROSPACE
TECHNICAL LIBRARY
ABBOTTAEROSPACE.COM

Table 5

SEMI-EMPIRICAL AND MEASURED OSCILLATORY CHORDWISE LOADINGS AT THREE SECTIONS

($M_\infty = 0.86$, $\bar{\nu} = 0.385$, $\alpha_0 = 2.07^\circ$, $\alpha_1 = 0.0058$ rad)

Semi-empirical values $\eta = 0.535$			Semi-empirical values $\eta = 0.766$			Semi-empirical values $\eta = 0.882$		
ξ	$\frac{\lvert\Delta\bar{C}_p\rvert}{\alpha_1}$	ε_Δ	ξ	$\frac{\lvert\Delta\bar{C}_p\rvert}{\alpha_1}$	ε_Δ	ξ	$\frac{\lvert\Delta\bar{C}_p\rvert}{\alpha_1}$	ε_Δ
0.027	14.31	-33.8	0.024	12.40	-31.2	0.026	13.70	-28.5
0.054	8.79	-31.7						
0.105	9.37	-28.6	0.107	9.50	-26.6	0.108	8.79	-23.7
0.156	9.46	-25.4	0.157	9.21	-23.9			
0.207	10.39	-22.5	0.208	9.36	-21.3	0.207	8.41	-18.6
0.308	11.51	-16.7	0.310	10.00	-16.3	0.311	10.53	-13.9
0.410	15.56	-12.0	0.411	8.94	-10.8	0.412	14.33	- 9.1
0.511	7.32	+ 0.6	0.512	5.97	- 1.6	0.513	5.22	+ 4.1
0.610	4.25	17.4	0.612	3.85	151.5	0.610	2.70	150.7
0.713	3.41	29.2	0.714	2.84	16.1	0.706	2.04	32.4
0.824	2.65	42.7	0.808	2.95	11.3	0.780	1.86	34.2
0.859	2.92	27.0	0.857	2.92	1.6	0.859	1.28	28.4

Measured values $\eta = 0.535$			Measured values $\eta = 0.766$			Measured values $\eta = 0.882$		
ξ	$\frac{\lvert\Delta\bar{C}_p\rvert}{\alpha_1}$	ε_Δ	ξ	$\frac{\lvert\Delta\bar{C}_p\rvert}{\alpha_1}$	ε_Δ	ξ	$\frac{\lvert\Delta\bar{C}_p\rvert}{\alpha_1}$	ε_Δ
0.025	10.62	-29.0						
			0.050	10.39	-28.9	0.050	9.06	-24.2
0.100	5.42	-25.2	0.100	7.62	-23.2	0.100	8.26	-21.4
0.150	6.52	-26.4	0.150	6.71	-20.5			
0.200	7.01	-25.8	0.200	6.66	-19.3	0.200	7.58	-27.2
0.300	12.11	-41.0	0.300	6.91	-27.2	0.300	8.51	-18.1
0.400	8.78	-39.5	0.400	10.94	-35.7	0.400	7.23	-21.5
0.500	5.28	-19.7	0.500	24.76	-13.1	0.500	14.96	+ 1.0
0.600	4.40	+17.5	0.600	5.12	+25.8	0.600	4.77	20.6
0.700	2.53	76.9	0.700	3.59	58.1	0.700	4.54	106.7
0.850	2.08	64.7	0.850	1.79	84.9	0.850	1.75	111.8

THIS DOCUMENT PROVIDED BY THE ABBOTT AEROSPACE
TECHNICAL LIBRARY
ABBOTTAEROSPACE.COM

Table 6

SEMI-EMPIRICAL AND MEASURED OSCILLATORY CHORDWISE LOADINGS FOR FOUR MACH NUMBERS (120 Hz, $\eta = 0.535$, $\alpha_0 = 2.07^{\circ}$, $\alpha_1 = 0.0058$ rad)

ξ	Semi-empirical $\lvert\Delta\bar{C}_p\rvert/\alpha_1$ for M_∞ =				Semi-empirical ε_Δ for M_∞ =			
	0.60	0.80	0.82	0.84	0.60	0.80	0.82	0.84
0.027	24.59	18.32	15.60	13.63	-22.1	-29.4	-30.6	-32.1
0.054	14.20	9.79	7.35	6.23	-20.0	-27.2	-28.4	-29.8
0.105	11.29	18.21	11.70	6.56	-16.7	-25.0	-26.0	-26.8
0.156	7.17	21.61	18.03	9.34	-11.5	-22.5	-23.8	-24.5
0.207	6.44	21.01	18.84	11.70	- 5.7	-19.4	-21.0	-22.0
0.308	4.71	5.19	14.25	17.01	+ 0.4	- 1.8	-13.8	-17.0
0.410	3.96	4.23	1.85	10.29	7.8	+ 7.3	+43.1	- 8.3
0.511	3.04	3.38	2.02	1.75	18.1	18.9	41.8	+54.1
0.610	2.12	2.84	1.95	1.76	36.5	30.5	50.9	100.5
0.713	2.44	2.97	1.92	1.70	23.7	30.3	59.4	81.6
0.824	1.64	2.28	1.94	1.83	49.2	47.7	68.5	79.5
0.859	1.44	2.22	1.93	1.79	39.3	39.8	50.0	60.0

ξ	Measured $\lvert\Delta\bar{C}_p\rvert/\alpha_1$ for M_∞ =				Measured ε_Δ for M_∞ =			
	0.60	0.80	0.82	0.84	0.60	0.80	0.82	0.84
0.025	22.89	16.09	15.02	12.91	-26.8	-21.5	-34.1	-34.6
0.100	10.43	17.96	11.72	5.88	-28.3	-32.8	-39.8	-34.3
0.150	6.89	26.21	9.95	9.08	-25.8	-39.6	-39.6	-40.5
0.200	5.20	11.99	22.55	12.73	-16.2	-23.3	-38.1	-49.6
0.300	3.69	8.16	15.37	16.88	- 5.4	+ 4.2	-27.1	-52.7
0.400	2.82	4.29	6.89	11.67	+ 1.5	27.5	+57.7	- 7.1
0.500	2.39	2.64	4.14	5.75	1.2	45.4	101.1	+25.8
0.600	1.41	2.12	3.12	4.06	28.4	55.0	96.9	82.2
0.700	0.98	1.47	2.72	3.17	58.2	78.7	117.9	101.4
0.850	1.66	0.86	1.42	1.69	48.8	96.7	72.2	92.2

THIS DOCUMENT PROVIDED BY THE ABBOTT AEROSPACE
TECHNICAL LIBRARY
ABBOTTAEROSPACE.COM

Table 7

IN-PHASE AND IN-QUADRATURE CHORDWISE LOADINGS AT $\eta = 0.766$ FOR FOUR MACH NUMBERS (120 Hz, $\alpha_0 = 2.07^\circ$, $\alpha_1 = 0.0058$ rad)

ξ	Semi-empirical $\Delta C_p'/\alpha_1$ for M_∞ =				Semi-empirical $\Delta C_p''/\alpha_1\bar{\nu}$ for M_∞ =			
	0.80	0.82	0.84	0.86	0.80	0.82	0.84	0.86
0.024	12.88	10.88	10.04	10.61	-16.28	-14.74	-14.59	-16.69
0.107	16.15	9.08	6.64	8.49	-17.39	-10.33	- 7.96	-11.03
0.157	26.73	13.73	7.16	8.42	-26.50	-14.36	- 7.69	- 9.68
0.208	21.18	21.28	9.02	8.73	-18.06	-20.35	- 8.76	- 8.81
0.310	3.92	24.74	15.39	9.60	+ 0.15	-18.03	-12.09	- 7.28
0.411	2.66	-0.71	15.21	8.78	1.60	+ 4.62	- 8.16	- 4.33
0.512	3.11	+0.44	1.78	5.96	1.82	3.81	+ 2.60	- 0.42
0.612	0.35	-1.91	-6.49	-3.38	3.63	5.08	6.73	+ 4.77
0.714	1.83	+0.65	-0.45	+2.73	2.91	3.81	3.60	2.05
0.808	1.61	0.63	+0.18	2.89	2.85	4.03	3.51	1.50
0.857	1.27	0.87	0.55	2.92	2.86	3.68	3.17	0.21

ξ	Measured $\Delta C_p'/\alpha_1$ for M_∞ =				Measured $\Delta C_p''/\alpha_1\bar{\nu}$ for M_∞ =			
	0.80	0.82	0.84	0.86	0.80	0.82	0.84	0.86
0.050	13.48	10.47	8.74	9.10	-22.08	-21.77	-22.52	-13.02
0.100	16.00	8.50	6.20	7.00	-22.80	-16.20	-12.70	- 7.80
0.150	17.81	8.24	5.51	6.28	-23.42	-15.02	-10.84	- 6.09
0.200	23.22	16.05	6.54	6.28	-28.50	-30.76	-11.98	- 5.72
0.300	6.01	19.43	10.12	6.15	+ 8.25	-29.24	-31.04	- 8.20
0.400	2.59	7.60	24.77	8.88	5.75	- 3.43	-37.83	-16.60
0.500	1.45	5.51	5.20	24.12	4.85	+ 2.44	+10.54	-14.53
0.600	-1.37	1.14	-2.63	4.61	5.01	4.51	16.82	+ 5.77
0.700	-0.15	1.53	-1.30	1.90	3.30	3.00	9.36	7.91
0.850	+0.07	-1.20	-0.97	0.16	1.73	- 0.21	3.04	4.64

THIS DOCUMENT PROVIDED BY THE ABBOTT AEROSPACE
TECHNICAL LIBRARY
ABBOTTAEROSPACE.COM

SYMBOLS

a	speed of sound
A	aspect ratio of wing; $2s/\bar{c}$
A_r	coefficient in equation (43)
c	local chord of wing
$\bar{c}$	geometric mean chord; reference length in Fig.1
C_{LLO}	mean local lift coefficient
$C_p(\alpha)$	pressure coefficient; $(p - p_\infty)\Big/\left(\frac{1}{2}\rho_\infty U_\infty^2\right)$
$\bar{C}_p$	$C'_p + iC''_p$; oscillatory pressure coefficient, e.g. equation (33)
G	local mean flow parameter in equation (13)
$\bar{H}$	complex integrand of equation (26); $\bar{J}U_\infty/(GU_0)$
$\bar{I}$	complex function in equation (21)
$\bar{J}$	complex function defined above equation (33)
$\bar{K}$	complex function in equation (22)
ℓ	steady non-dimensional loading ΔC_p from linear theory
$\bar{\ell}$	$\ell' + i\ell''$; loading coefficient from linear theory in equation (17)
M	Mach number; U/a
N	number of terms in linear chordwise loading
p	static pressure
q	integer $1(1)N$ denoting term in chordwise loading
$\Re$	real part of
s	semi-span of wing in Fig.1
t	time
U	speed
x	ordinate in streamwise direction
x_a	local ordinate of swept axis in Fig.1
x_L	local ordinate of leading edge
y	spanwise distance from centre line
z	upward vertical displacement
α	incidence of wing at crank station $\eta = 0.319$ (in radians unless otherwise stated)
α_0	mean value of α
α_1	amplitude of oscillation in equation (30)
γ	ratio of specific heats of air (= 1.4)
Γ_q	steady spanwise loading function in equation (17) with $\omega = 0$
$\bar{\Gamma}_q$	complex spanwise loading function in equation (17) from Ref.3

THIS DOCUMENT PROVIDED BY THE ABBOTT AEROSPACE
TECHNICAL LIBRARY
ABBOTTAEROSPACE.COM

SYMBOLS (concluded)

ΔC_p	non-dimensional local loading coefficient; $C_{p\ell} - C_{pu}$
$\Delta \bar{C}_p$	$\Delta C'_p + i\Delta C''_p$; oscillatory loading coefficient
$\lvert\Delta \bar{C}_p\rvert$	amplitude of $\Delta \bar{C}_p$ in equation (36)
ε_Δ	phase lead of $\Delta \bar{C}_p$ in equation (37)
η	non-dimensional spanwise distance; y/s
$\bar{\nu}$	frequency parameter; $\omega \bar{c}/U_\infty$
ξ	non-dimensional chordwise distance in equation (18)
ρ	air density
ϕ	angular chordwise parameter in equation (18)
Φ	velocity potential
$\bar{\Phi}$	complex oscillatory velocity potential
ψ	periodic variable; ωt
ω	circular frequency of oscillation
0	subscript denoting mean steady flow at $\alpha = \alpha_0$
1	subscript denoting amplitude $\alpha = \alpha_1$
∞	subscript denoting undisturbed stream
ℓ	subscript denoting lower surface
u	subscript denoting upper surface
lin	subscript denoting linear theory
$\bar{\nu} = 0$	subscript denoting steady flow

THIS DOCUMENT PROVIDED BY THE ABBOTT AEROSPACE
TECHNICAL LIBRARY
ABBOTTAEROSPACE.COM

REFERENCES

No.	Author	Title, etc.
1	N.C. Lambourne H.C. Garner B.L. Welsh	Some measurements of oscillatory loading and related semi-empirical predictions on a wing in supercritical flow. RAE Technical Memorandum Aero 1541 (1973)
2	N.C. Lambourne B.L. Welsh	Pressure measurements on a wing oscillating in super-critical flow. RAE Technical Report to be issued
3	Doris E. Lehrian H.C. Garner	Theoretical calculation of generalized forces and load distribution on wings oscillating at general frequency in a subsonic stream. ARC R&M 3710 (1971)
4	E. Albano W.P. Rodden	A doublet-lattice method for calculating lift distributions on oscillating surfaces in subsonic flows. AIAA Journal, Vol.7, No.2, pp.279-285 (1969)
5	D.J. Allen D.S. Sadler	Oscillatory aerodynamic forces in linearised supersonic flow for arbitrary frequencies, planforms and Mach numbers. ARC R&M 3415 (1963)
6	M.T. Landahl	Unsteady Transonic Flow Theory. Pergamon Press (1961)
7	D.E. Davies	Three-dimensional sonic theory. Manual on Aeroelasticity, Vol.2, Ch.4, AGARD (Ed. W.P. Jones) (1960)
8	H.C. Garner Doris E. Lehrian	Comparative theoretical calculations of forces on oscillating wings through the transonic speed range. ARC R&M 3559 (1967)
9	H. Bergh R.J. Zwaan	A method for estimating unsteady pressure distributions for arbitrary vibration modes from theory and from measured distributions for one single mode. NLR (Netherlands) Report TR F.250 (1966)
10	S.R. Bland	Comments on NASA Langley research on transonic unsteady aerodynamics. AGARD Report 611 (1973)

THIS DOCUMENT PROVIDED BY THE ABBOTT AEROSPACE
TECHNICAL LIBRARY
ABBOTTAEROSPACE.COM

REFERENCES (concluded)

No.	Author	Title, etc.
11	H. Tijdeman R.J. Zwaan	On the prediction of aerodynamic loads on oscillating wings in transonic flow. AGARD Report 612 (1973)
12	E.M. Murman J.D. Cole	Calculation of plane steady transonic flows. AIAA Journal, Vol.9, No.1, pp.121-141 (1971)
13	F.E. Ehlers	A finite difference method for the solution of the transonic flow around harmonically oscillating wings. NASA CR-2257 (1974)
14	C.M. Albone D. Catherall M.G. Hall M.G. Joyce	An improved numerical method for solving the transonic small-perturbation equation for the flow past a lifting aerofoil. RAE Technical Report 74056 (1974)
15	R.C. Lock	Research in the UK on finite difference methods for computing steady transonic flows. Symposium Transsonicum II, Göttingen, 8-13 September 1975, pp.457-486, Springer-Verlag (1976)
16	A.M. Cunningham	The application of general aerodynamic lifting surface elements to problems in unsteady transonic flow. NASA CR-112264 (1973)
17	S.S. Stahara J.R. Spreiter	Development of a nonlinear unsteady transonic flow theory. NASA CR-2258 (1973)
18	J.D. Revell	Research on unsteady transonic flow theory. NASA CR-112114 (1973)
19	S.Y. Ruo J.G. Theisen	Calculation of unsteady transonic aerodynamics for oscillating wings with thickness. NASA CR-2259 (1973)
20	H.C. Garner	Low-speed theoretical and experimental aerodynamic loading on highly-swept curved-tipped wings of two thicknesses. RAE Technical Report 72177 (ARC R&M 3735) (1972)
21	W.F. Ballhaus F.R. Bailey	Numerical calculation of transonic flow about swept wings. AIAA Paper 72-677 (1972)

THIS DOCUMENT PROVIDED BY THE ABBOTT AEROSPACE
TECHNICAL LIBRARY
ABBOTTAEROSPACE.COM

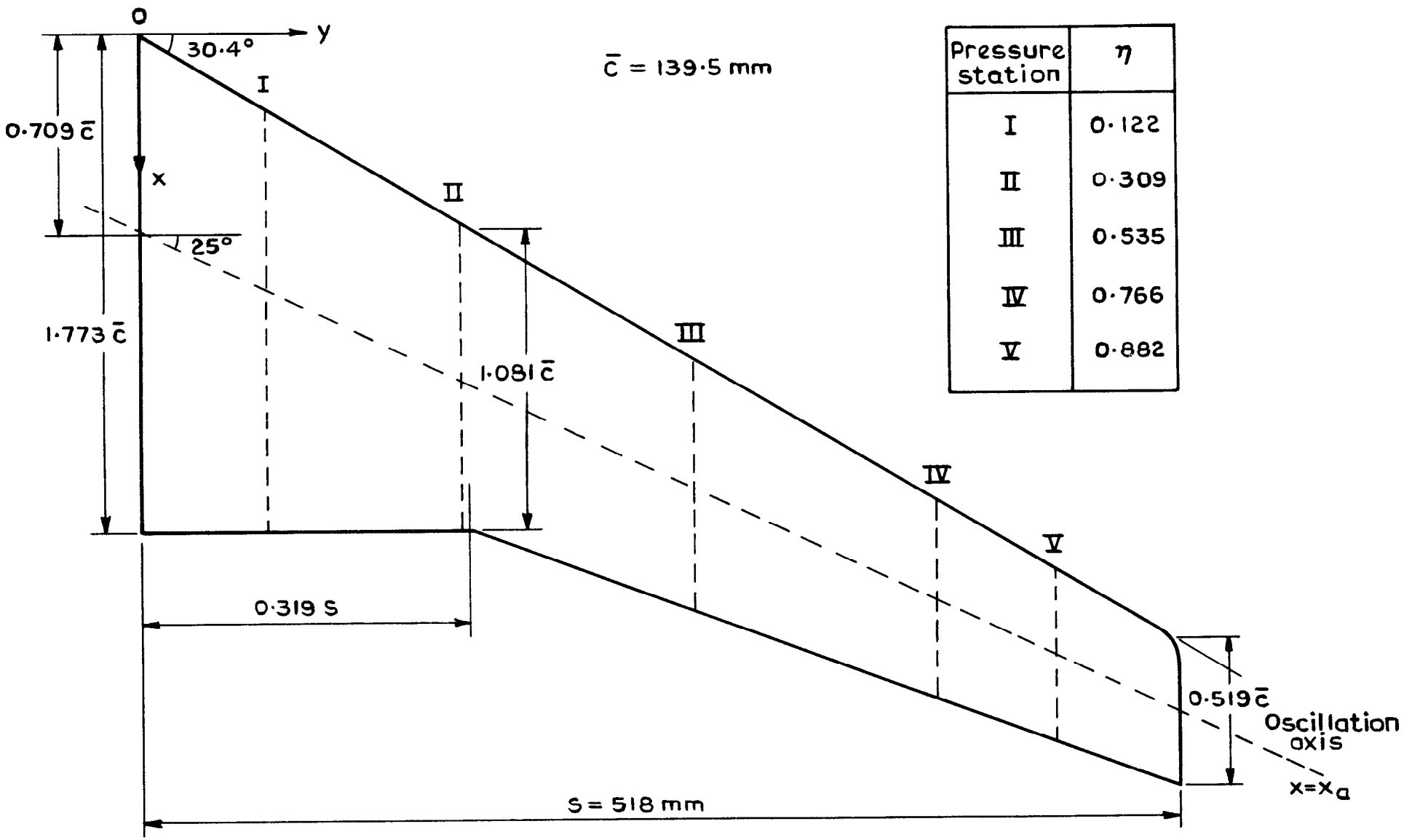

Pressure station	η
I	0·122
II	0·309
III	0·535
IV	0·766
V	0·882

Fig.1 Details of model planform, pressure stations and oscillation axis

THIS DOCUMENT PROVIDED BY THE ABBOTT AEROSPACE
TECHNICAL LIBRARY
ABBOTTAEROSPACE.COM

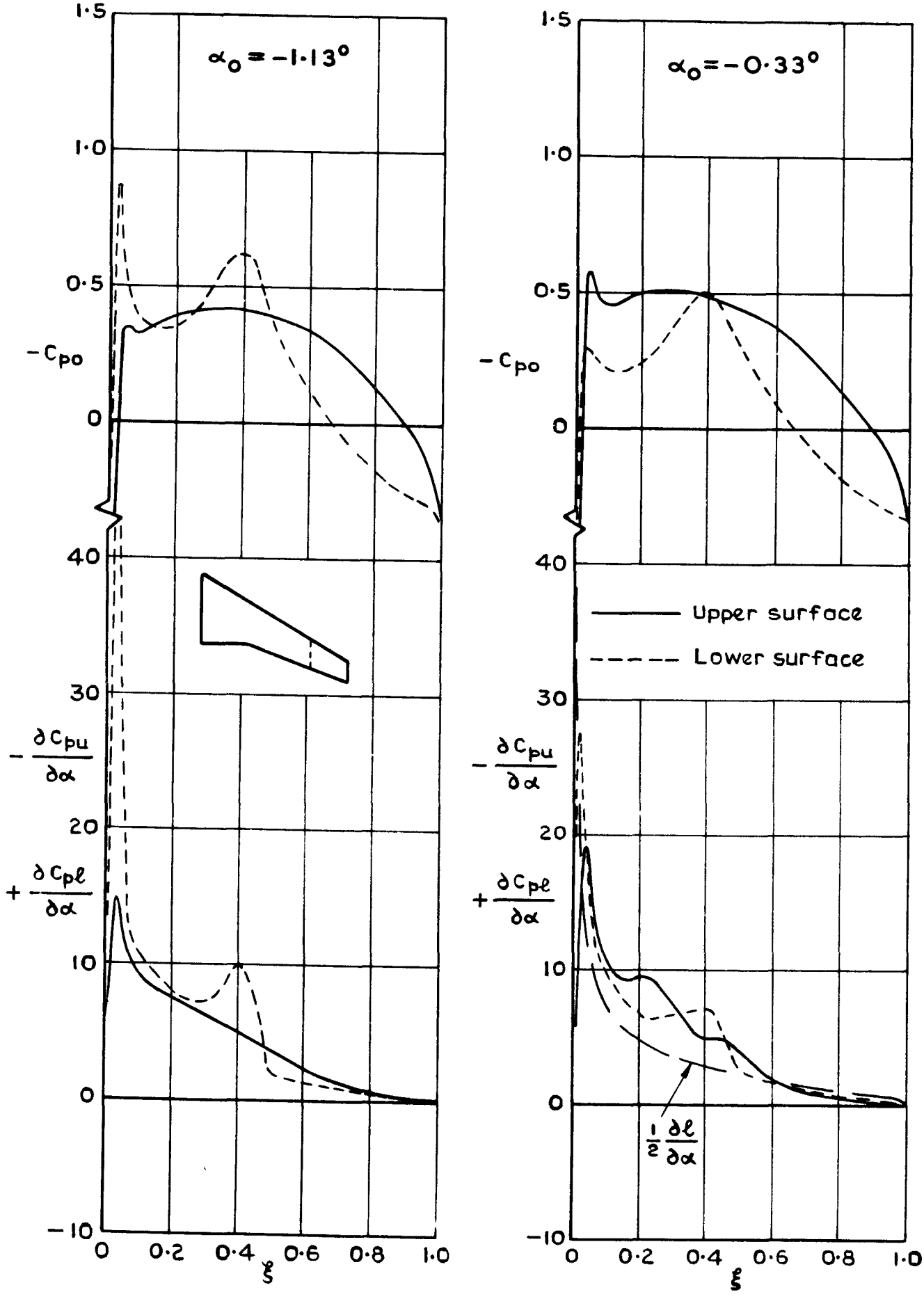

Fig. 2 Transonic small-perturbation theory ($M_\infty = 0.84$, $\eta = 0.750$)

This Document Provided by the Abbott Aerospace
TECHNICAL LIBRARY
ABBOTTAEROSPACE.COM

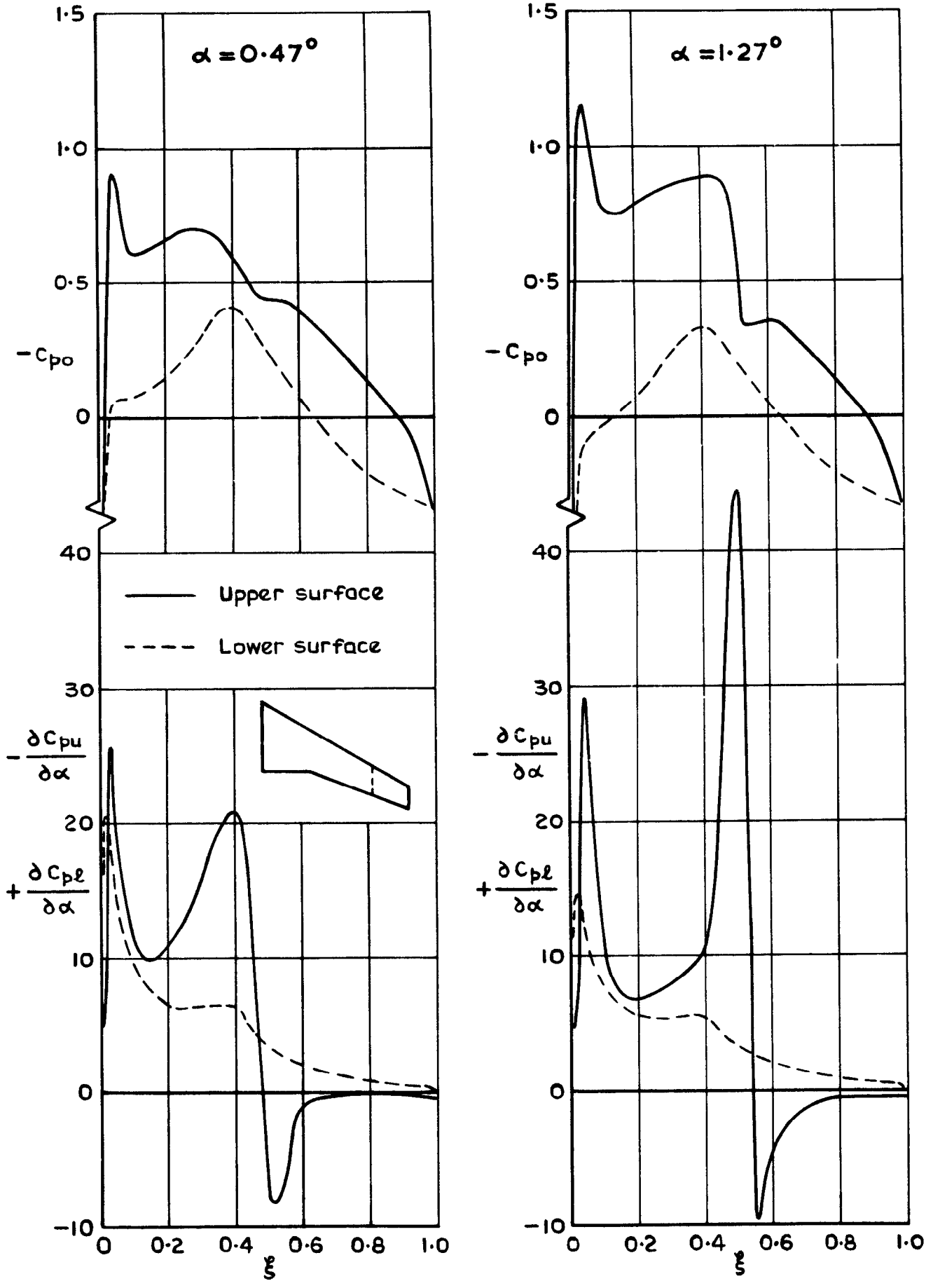

Fig. 3 Transonic small-perturbation theory ($M_\infty = 0{\cdot}84$, $\eta = 0{\cdot}750$)

THIS DOCUMENT PROVIDED BY THE ABBOTT AEROSPACE
TECHNICAL LIBRARY
ABBOTTAEROSPACE.COM

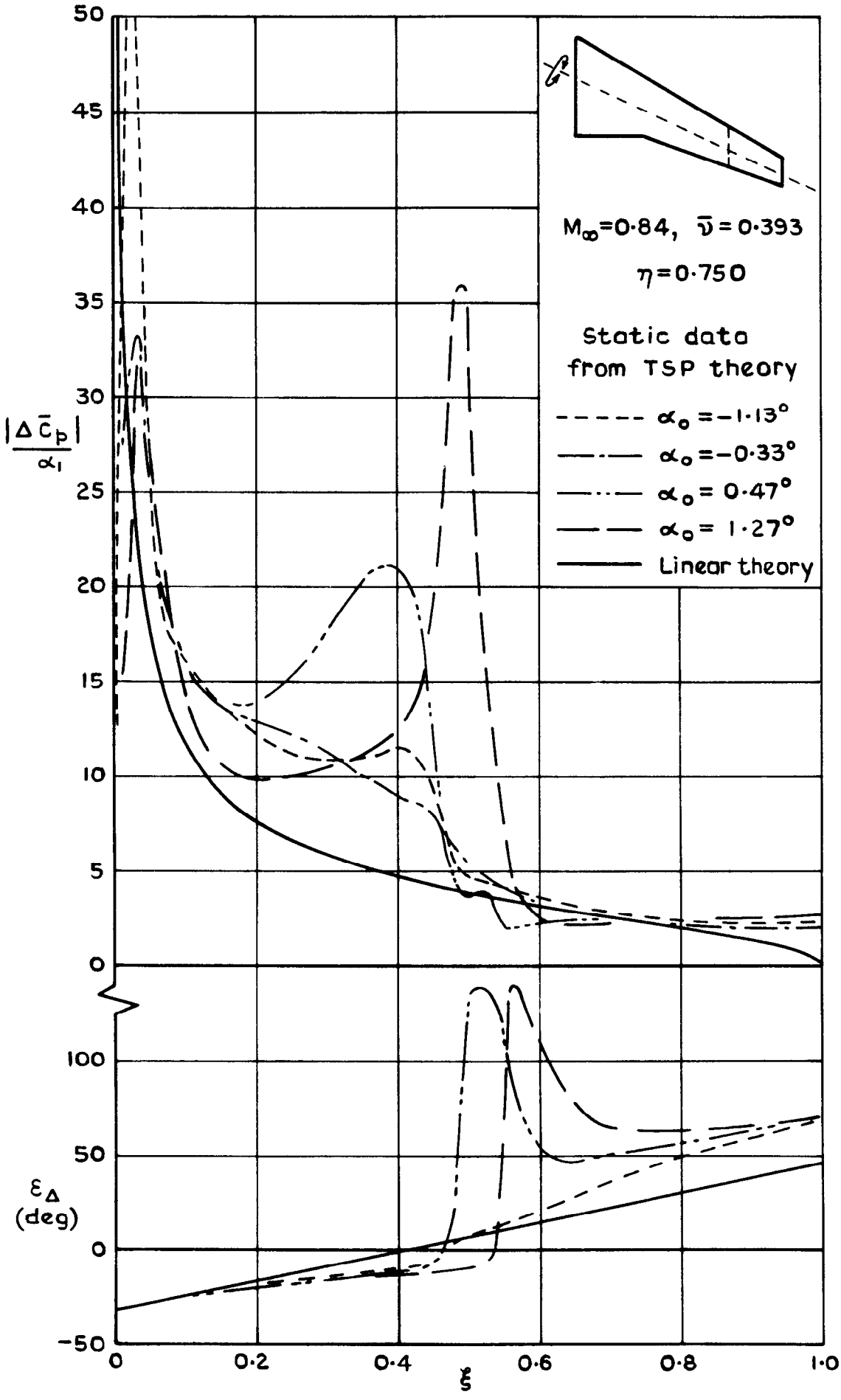

Fig.4 Effect of mean incidence on amplitude and phase of oscillatory loading

THIS DOCUMENT PROVIDED BY THE ABBOTT AEROSPACE
TECHNICAL LIBRARY
ABBOTTAEROSPACE.COM

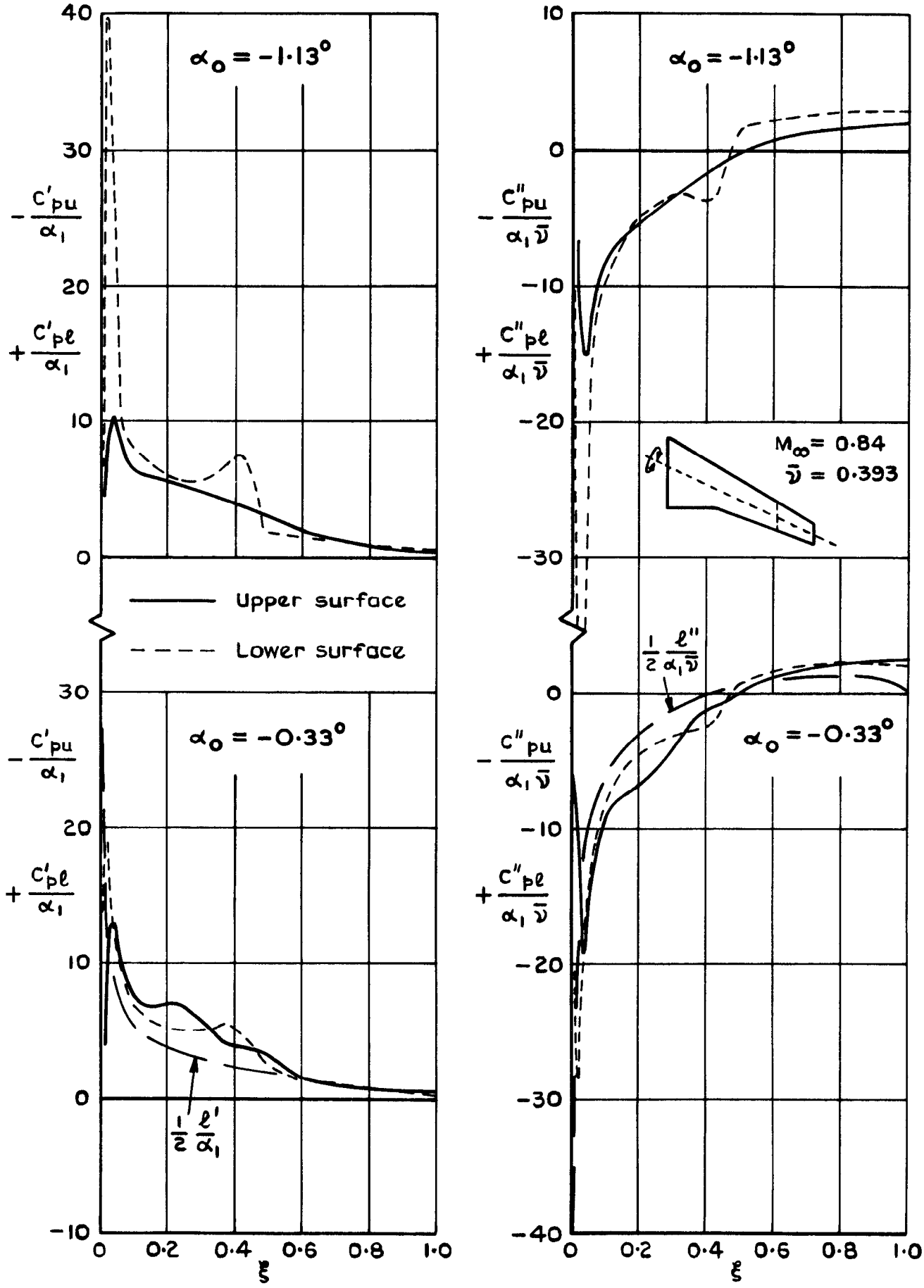

Fig.5 Calculated oscillatory pressures on upper and lower surfaces at $\eta = 0{\cdot}750$

THIS DOCUMENT PROVIDED BY THE ABBOTT AEROSPACE
TECHNICAL LIBRARY
ABBOTTAEROSPACE.COM

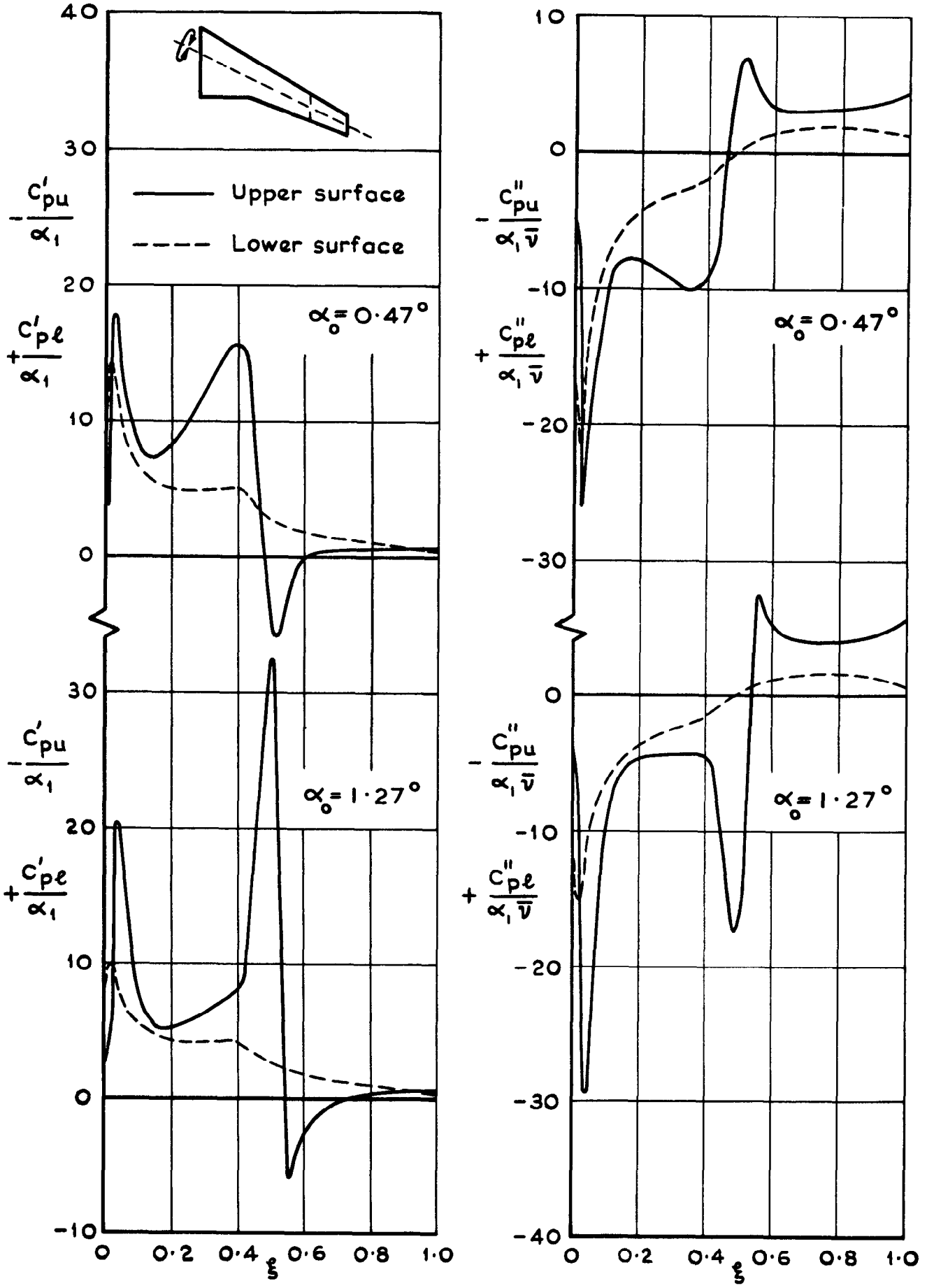

Fig.6 Calculated oscillatory pressures on upper and lower surfaces at $\eta = 0{\cdot}750$

THIS DOCUMENT PROVIDED BY THE ABBOTT AEROSPACE
TECHNICAL LIBRARY
ABBOTTAEROSPACE.COM

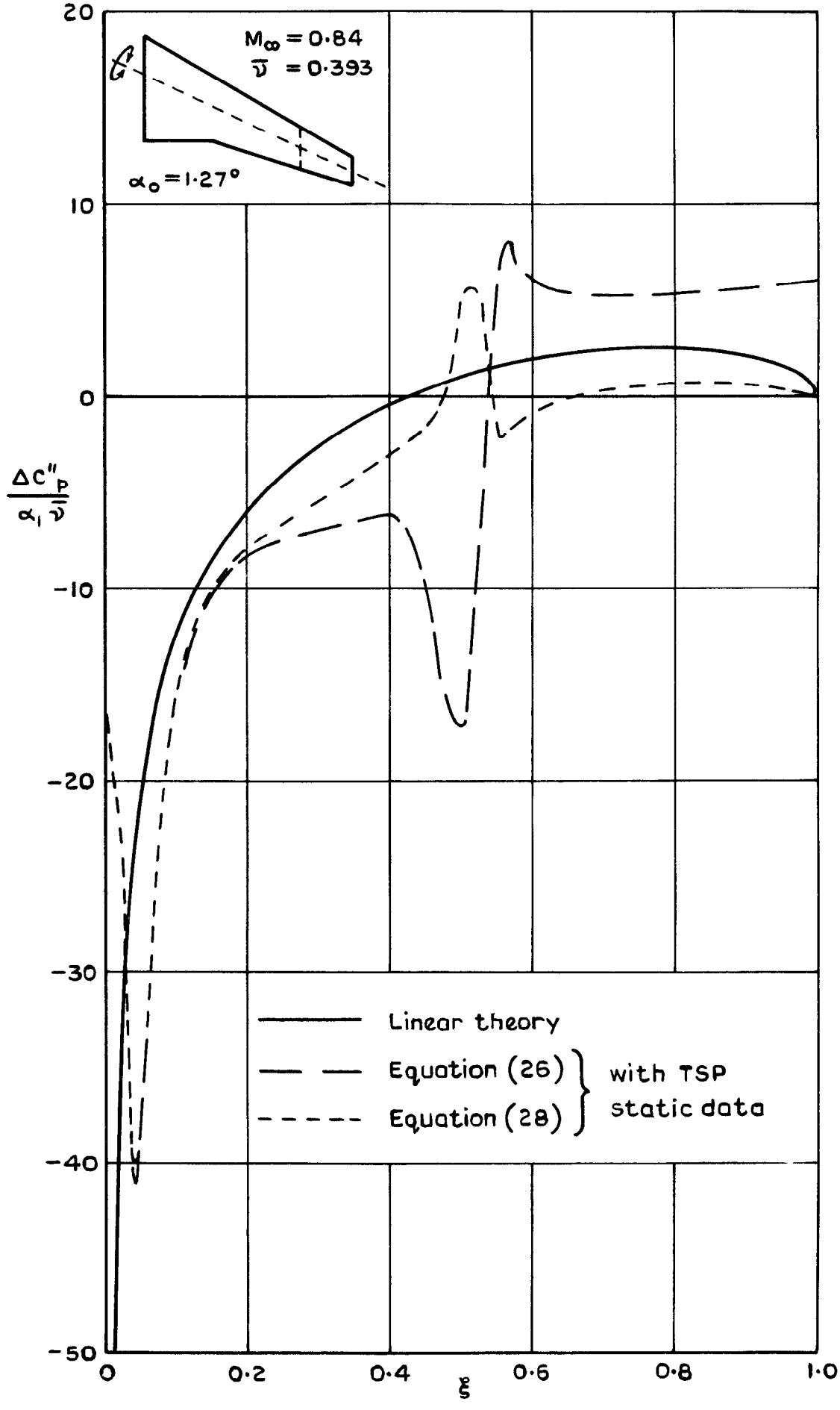

Fig.7 Various calculations of in-quadrature loading at $\eta = 0.750$

THIS DOCUMENT PROVIDED BY THE ABBOTT AEROSPACE
TECHNICAL LIBRARY
ABBOTTAEROSPACE.COM

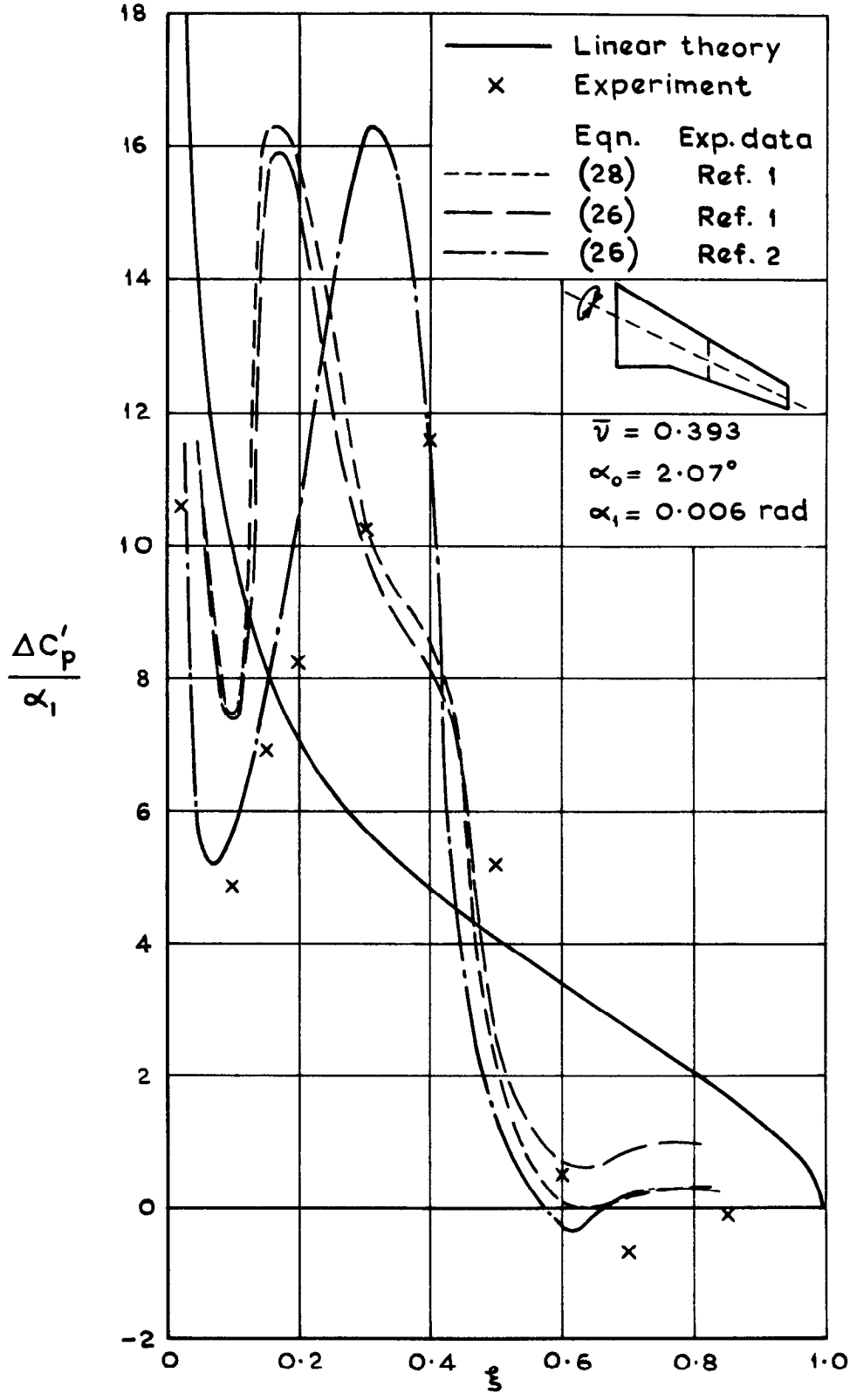

Fig.8 Measured and semi-empirically calculated in-phase chordwise loading at $\eta = 0{\cdot}535$ and $M_\infty = 0{\cdot}84$

THIS DOCUMENT PROVIDED BY THE ABBOTT AEROSPACE
TECHNICAL LIBRARY
ABBOTTAEROSPACE.COM

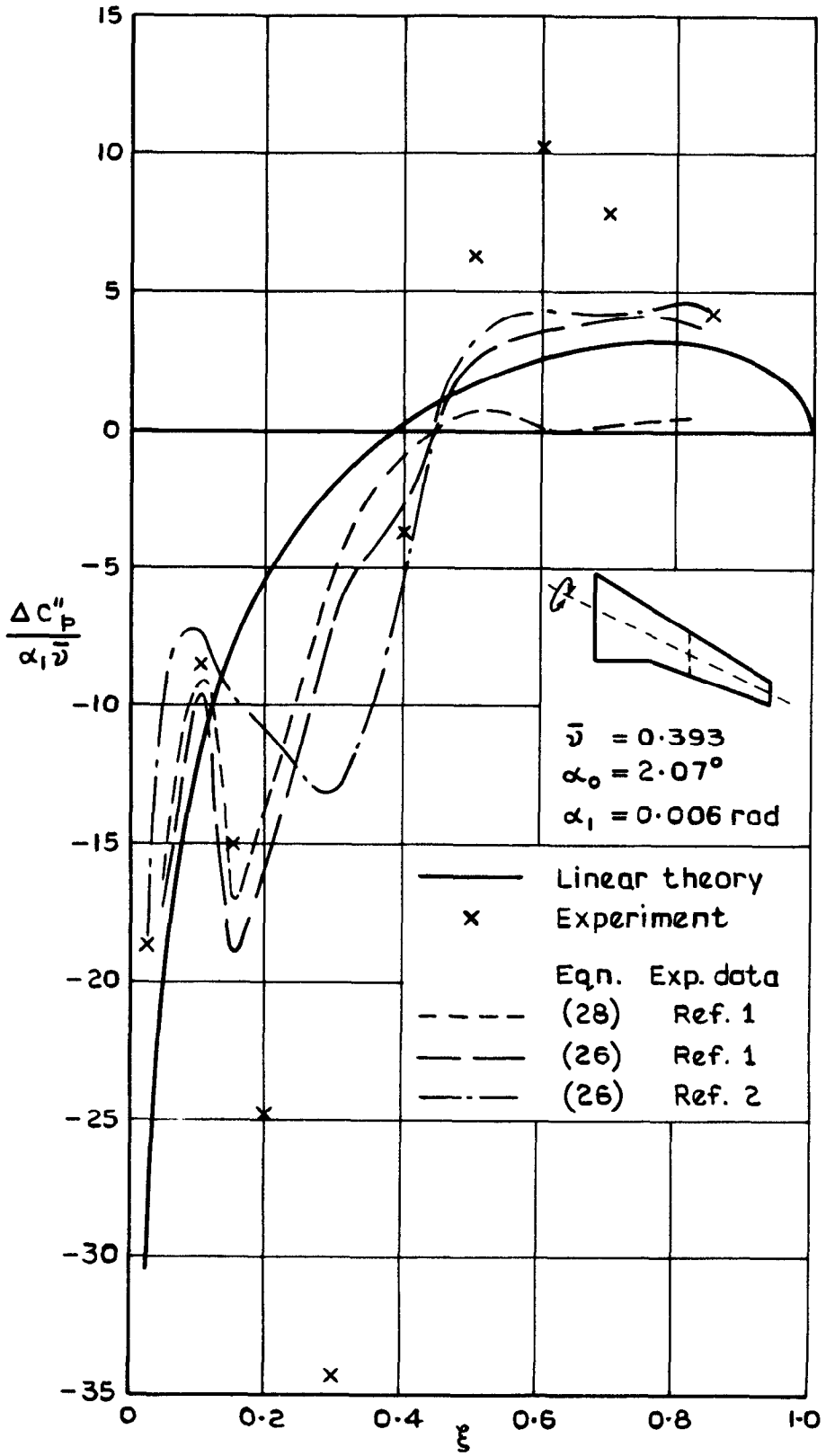

Fig.9 Measured and semi-empirically calculated in-quadrature chordwise loading at η=0·535 and M_∞= 0·84

THIS DOCUMENT PROVIDED BY THE ABBOTT AEROSPACE
TECHNICAL LIBRARY
ABBOTTAEROSPACE.COM

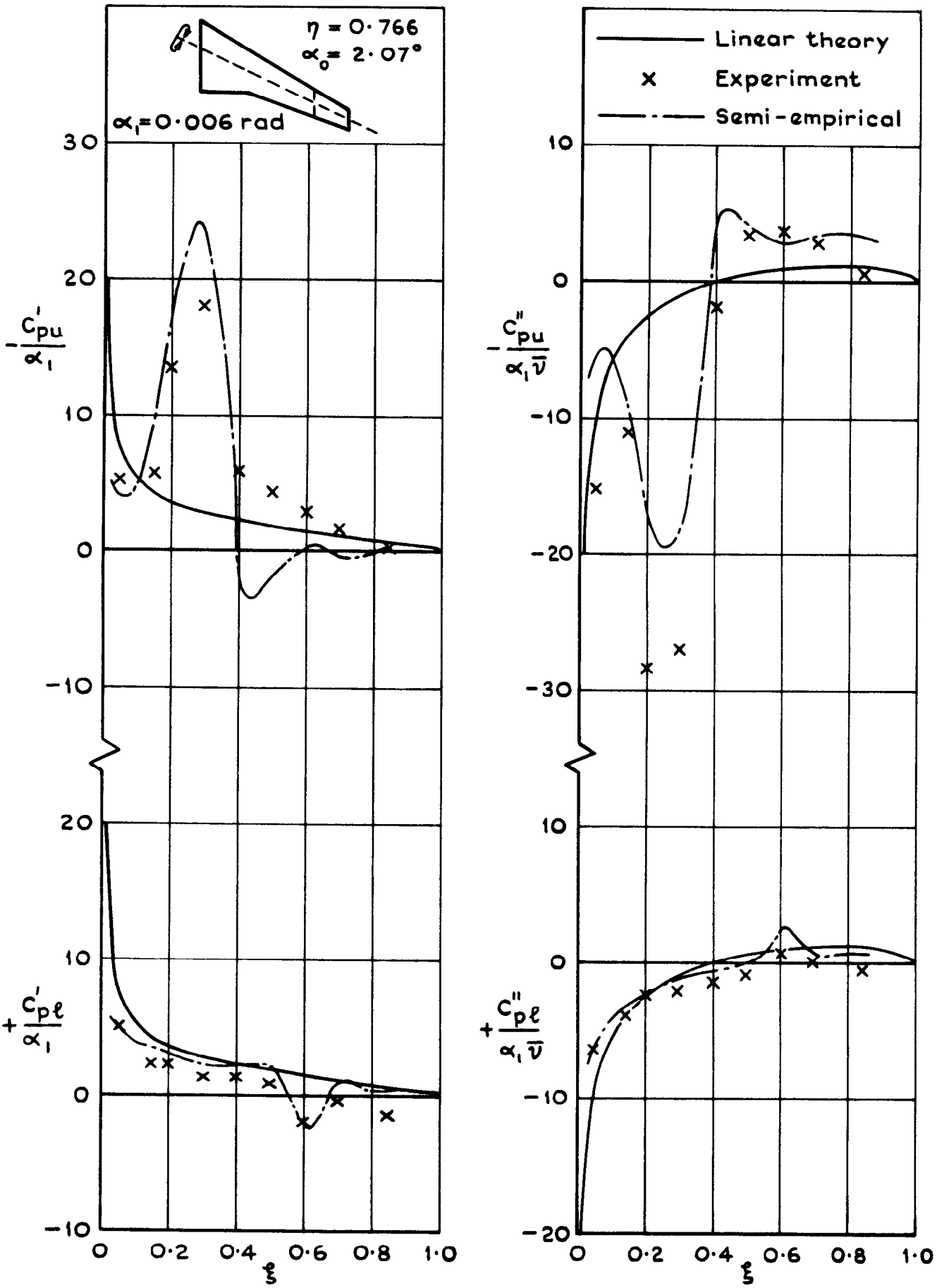

Fig.10 Measured and calculated oscillatory surface pressures ($M_\infty = 0{\cdot}82$, $\bar{\nu} = 0{\cdot}402$)

THIS DOCUMENT PROVIDED BY THE ABBOTT AEROSPACE
TECHNICAL LIBRARY
ABBOTTAEROSPACE.COM

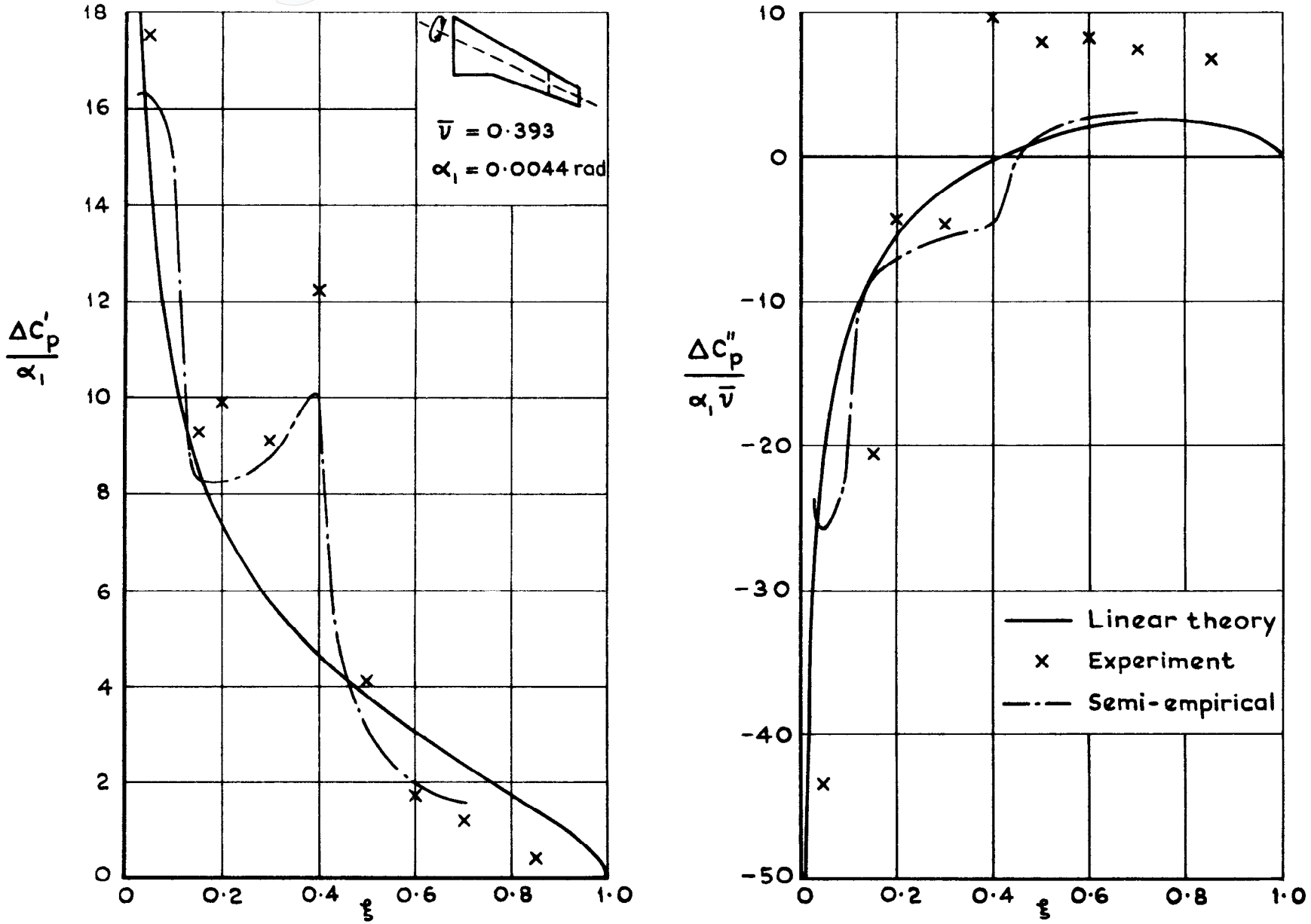

Fig.11 Calculated and measured oscillatory chordwise loading
($M_\infty = 0.84$, $\eta = 0.766$, $\alpha_0 = -1.28^\circ$)

THIS DOCUMENT PROVIDED BY THE ABBOTT AEROSPACE
TECHNICAL LIBRARY
ABBOTTAEROSPACE.COM

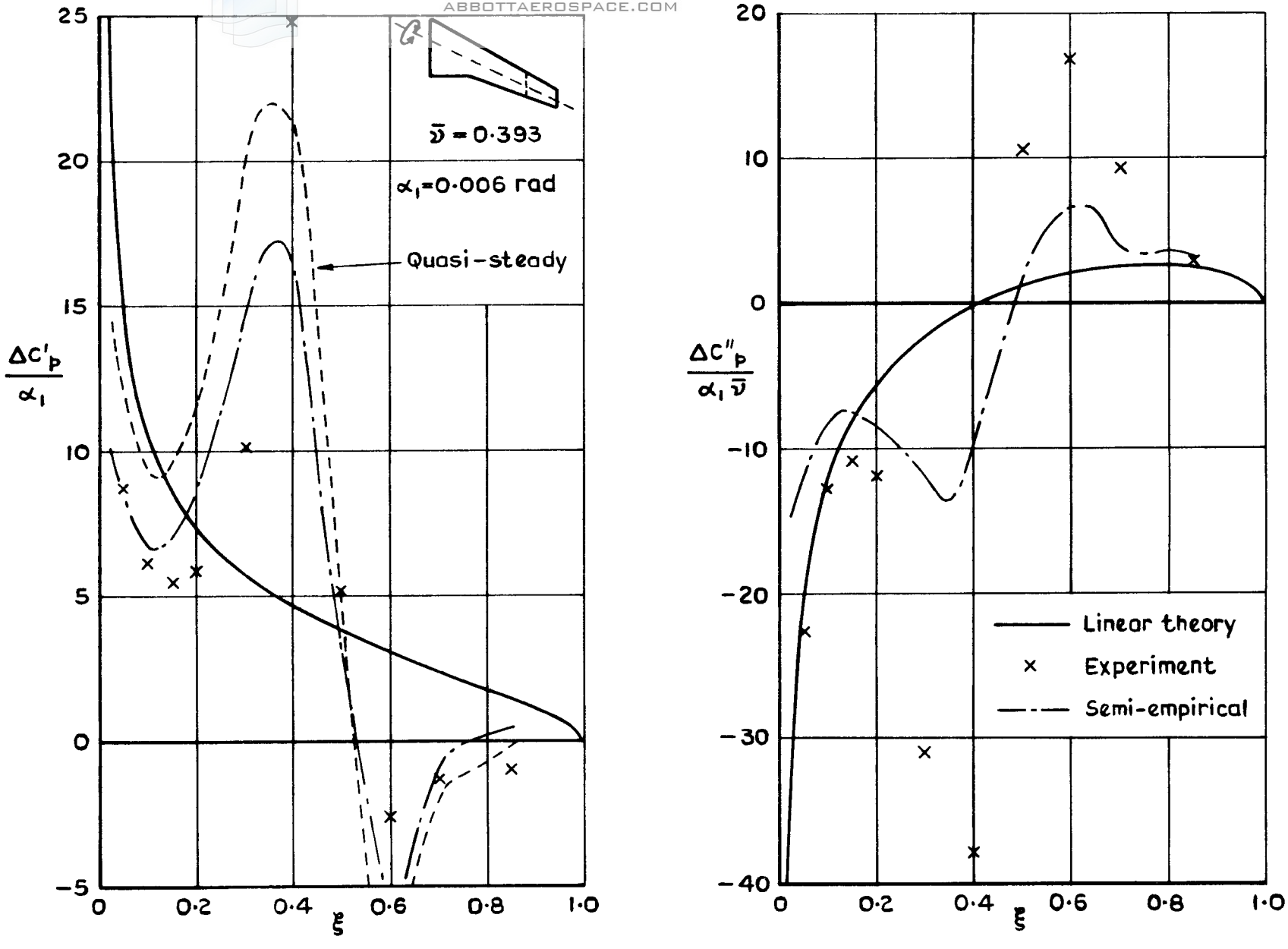

Fig.12 Calculated and measured oscillatory chordwise loading
($M_\infty = 0.84$, $\eta = 0.766$, $\alpha_0 = 2.07^\circ$)

THIS DOCUMENT PROVIDED BY THE ABBOTT AEROSPACE
TECHNICAL LIBRARY
ABBOTTAEROSPACE.COM

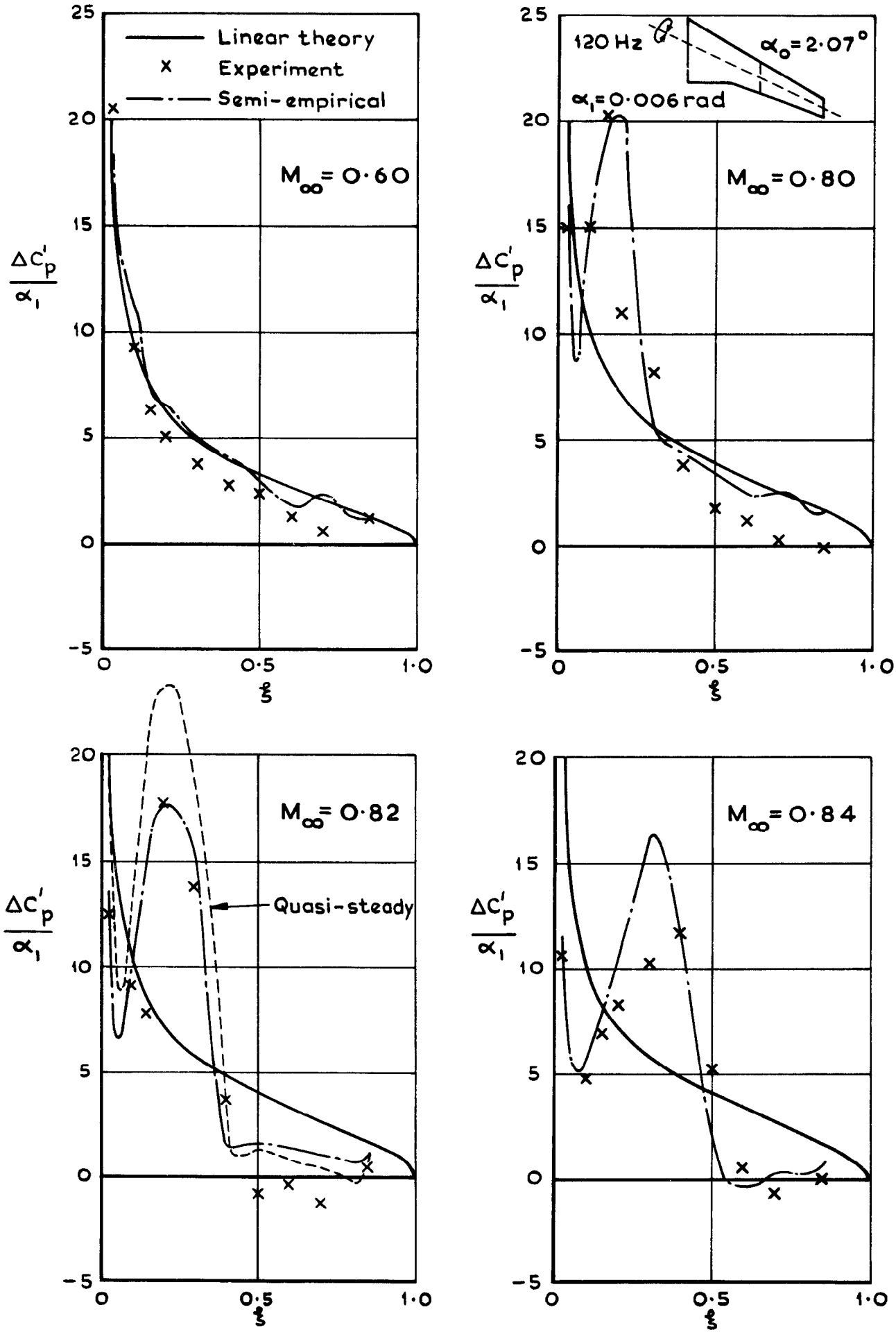

Fig.13 In-phase chordwise loading at $\eta = 0{\cdot}535$ for four Mach numbers

THIS DOCUMENT PROVIDED BY THE ABBOTT AEROSPACE
TECHNICAL LIBRARY
ABBOTTAEROSPACE.COM

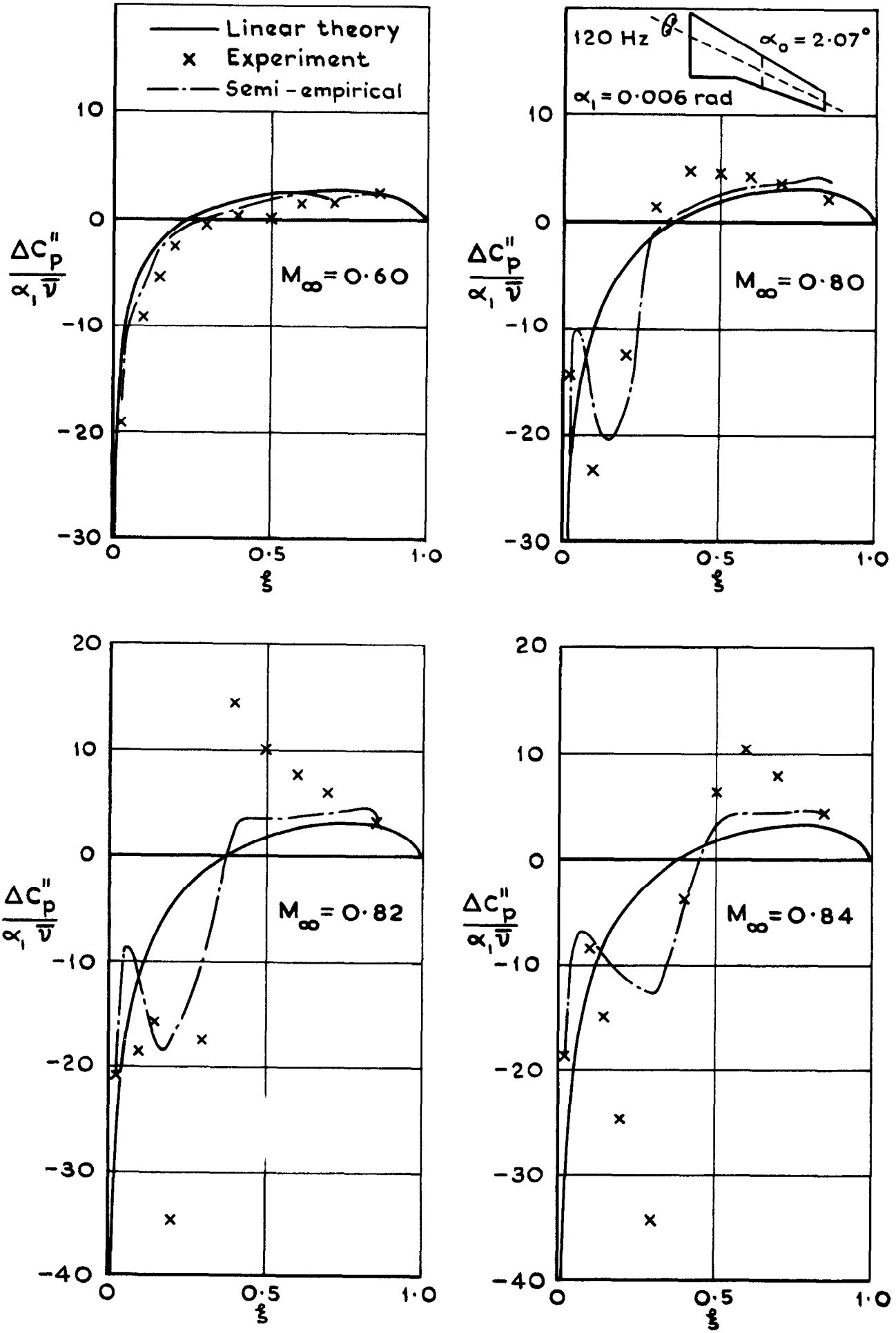

Fig.14 In-quadrature chordwise loading at $\eta = 0{\cdot}535$ for four Mach numbers

THIS DOCUMENT PROVIDED BY THE ABBOTT AEROSPACE
TECHNICAL LIBRARY
ABBOTTAEROSPACE.COM

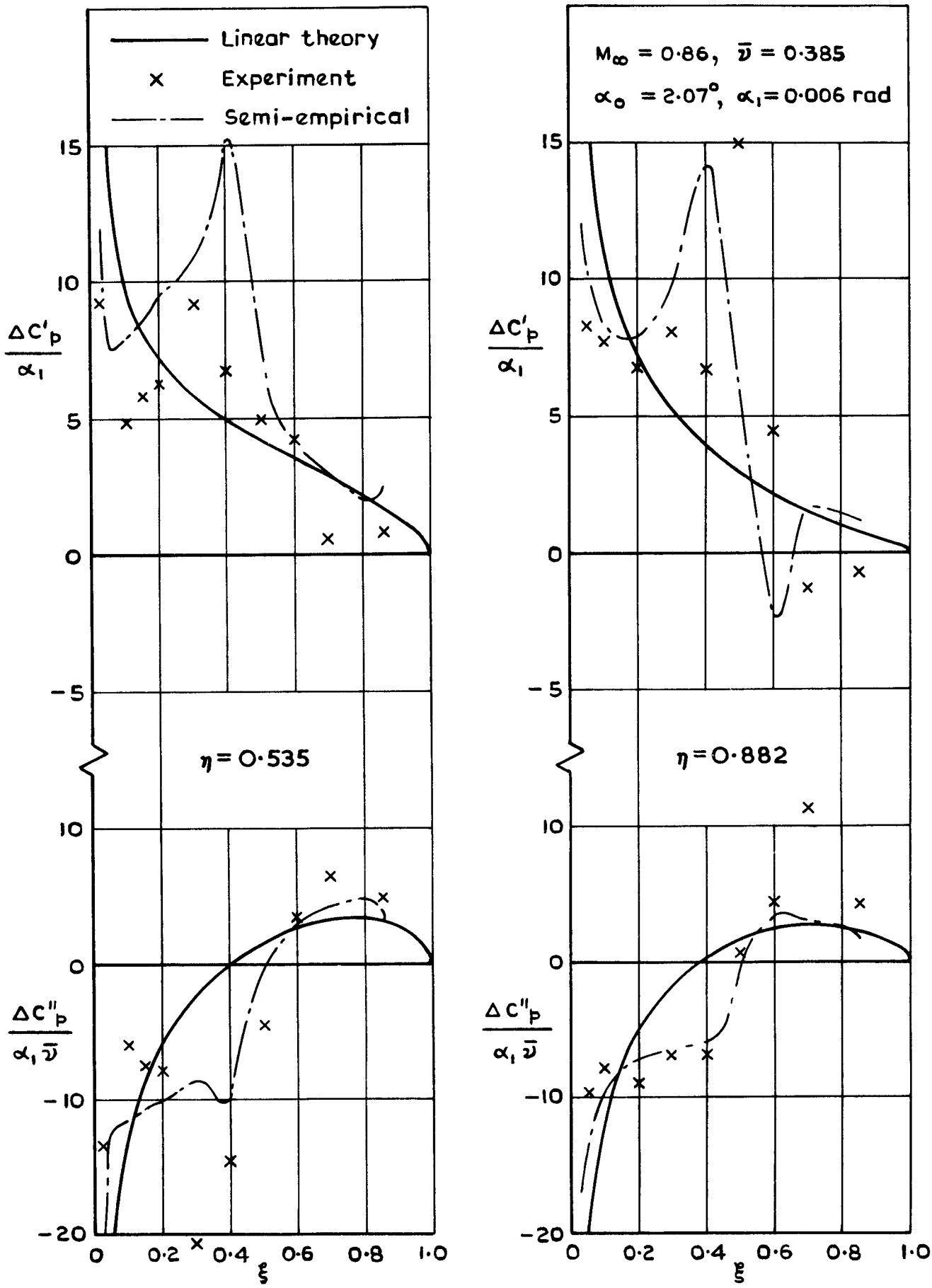

Fig.15 Calculated and measured oscillatory loading at two sections

THIS DOCUMENT PROVIDED BY THE ABBOTT AEROSPACE
TECHNICAL LIBRARY
ABBOTTAEROSPACE.COM

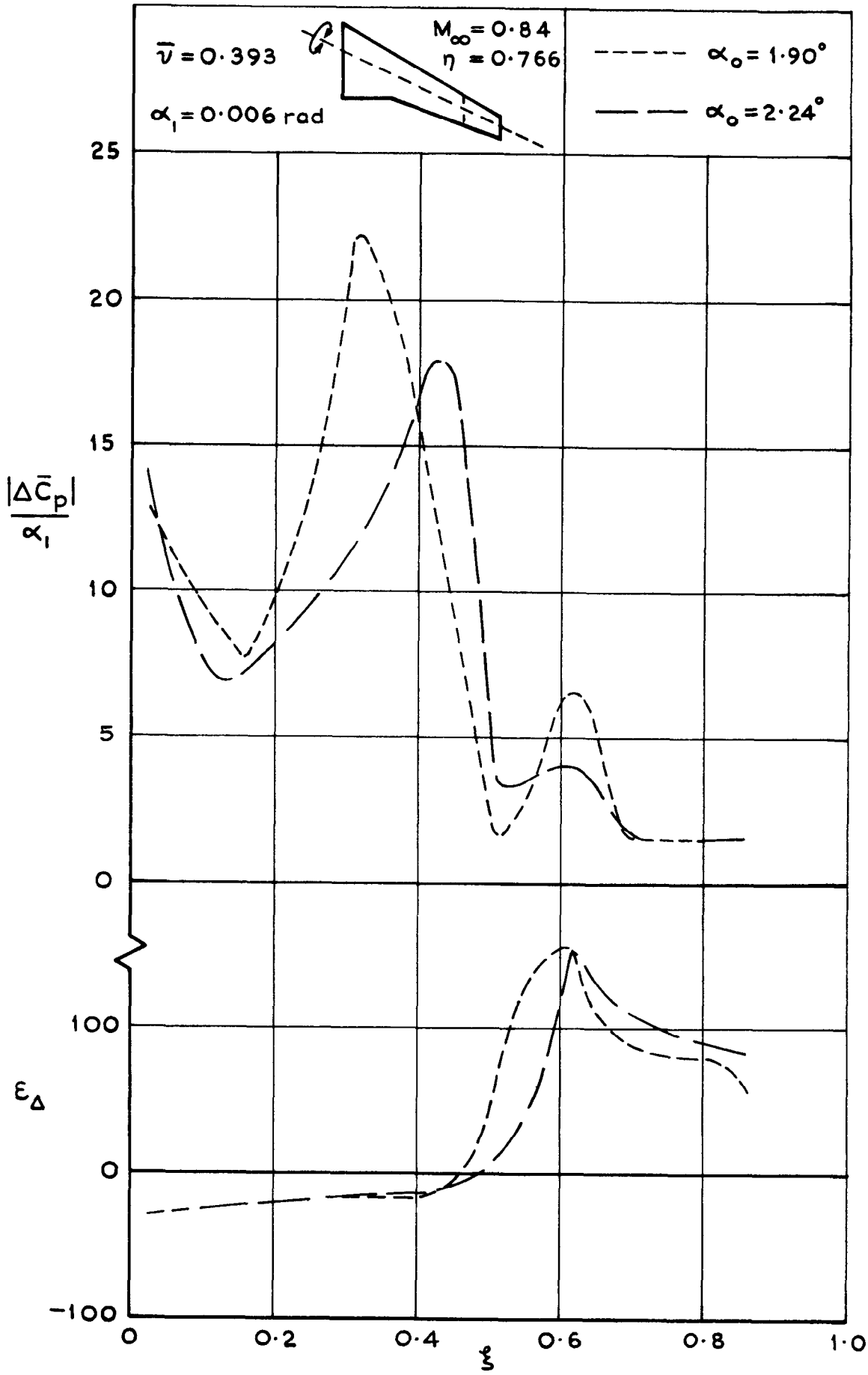

Fig.16 Semi-empirical effects of mean incidence on oscillatory loading

THIS DOCUMENT PROVIDED BY THE ABBOTT AEROSPACE
TECHNICAL LIBRARY
ABBOTTAEROSPACE.COM

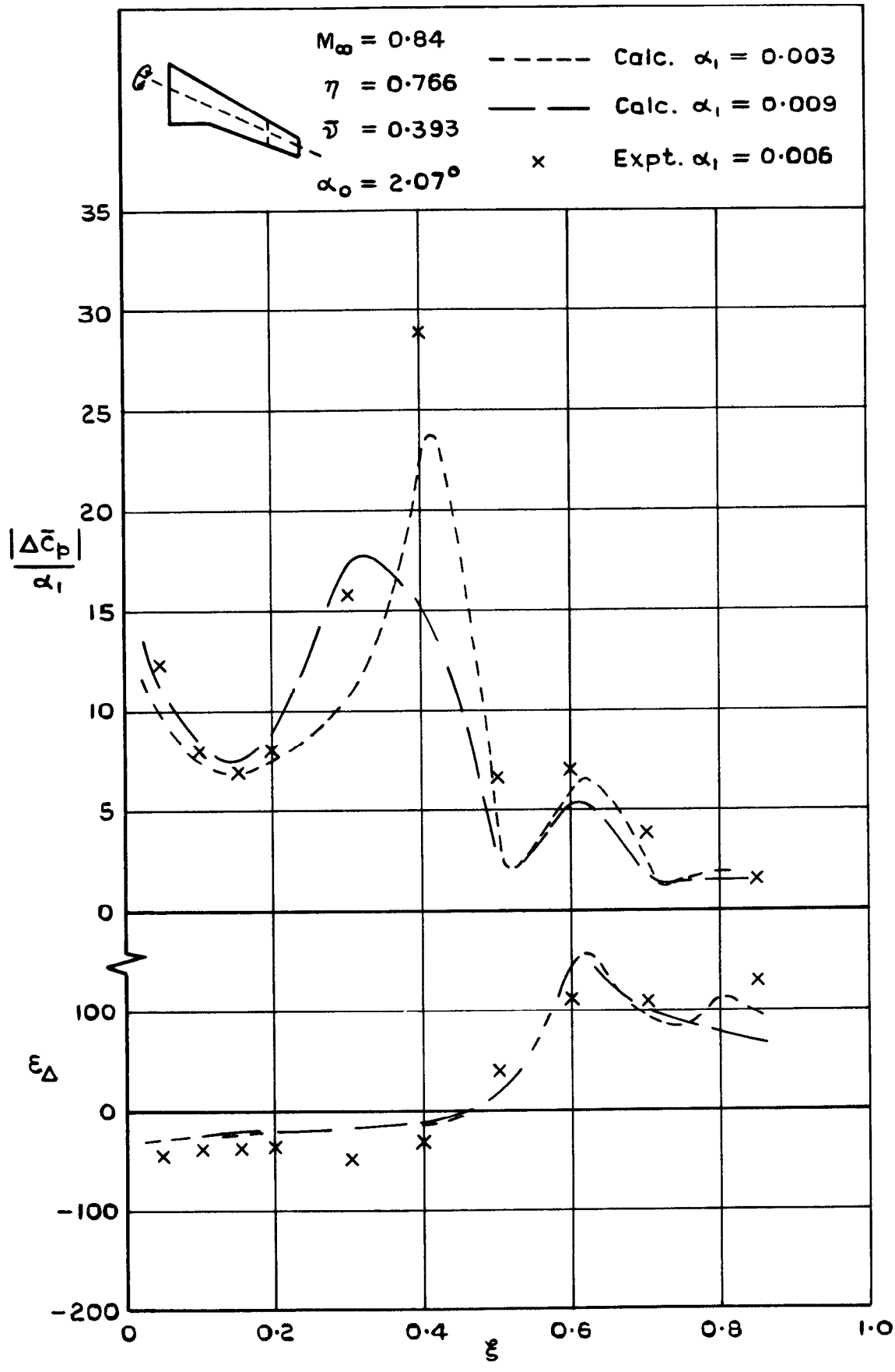

Fig. 17 Semi-empirical effects of amplitude on oscillatory loading

THIS DOCUMENT PROVIDED BY THE ABBOTT AEROSPACE
TECHNICAL LIBRARY
ABBOTTAEROSPACE.COM

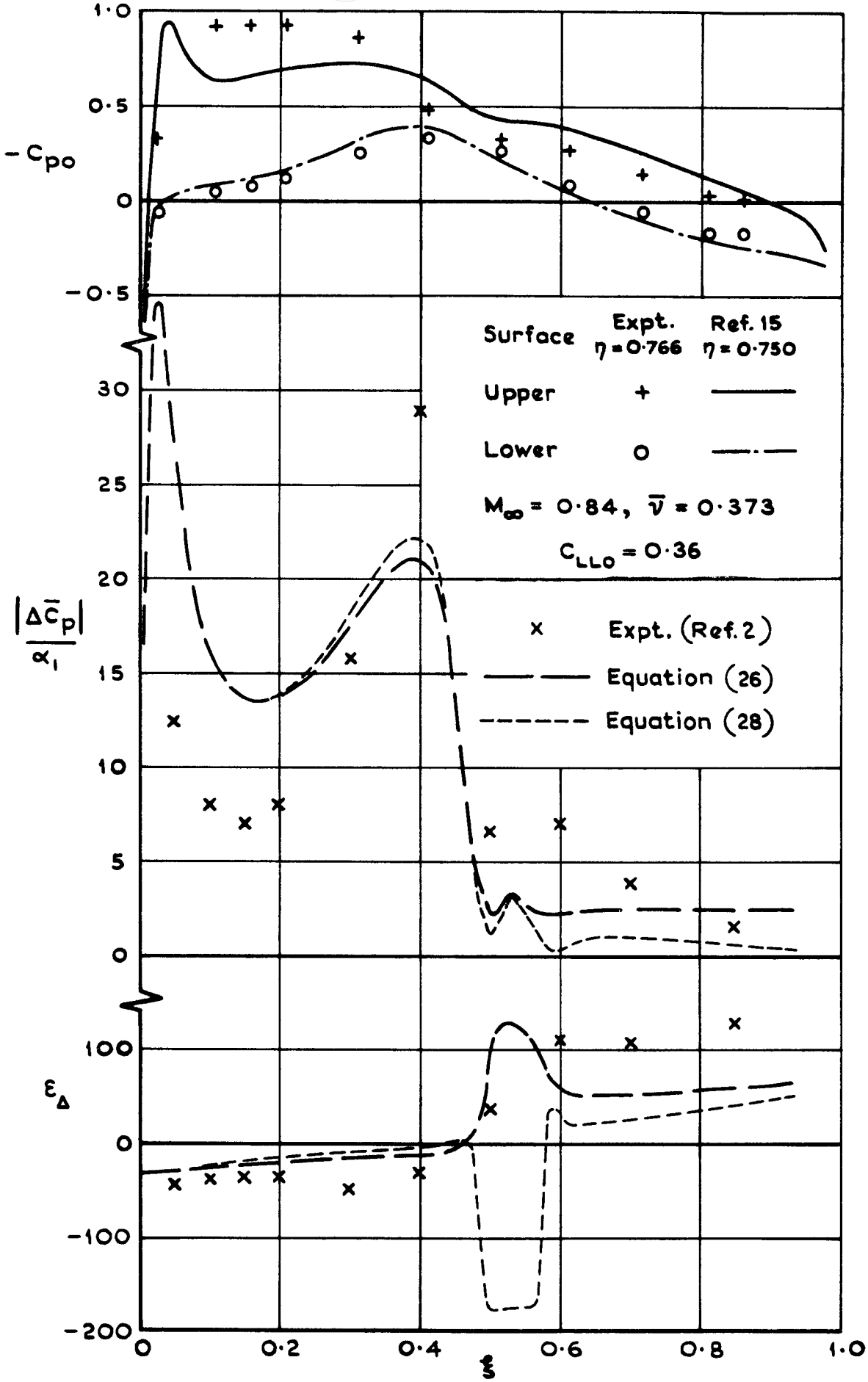

Fig.18 Chordwise distributions of mean pressure and oscillatory loading as measured and calculated with static data from TSP theory

Printed in England for Her Majesty's Stationery Office by the Royal Aircraft Establishment, Farnborough Dd. 290279 K5 10/76.

THIS DOCUMENT PROVIDED BY THE ABBOTT AEROSPACE
TECHNICAL LIBRARY
ABBOTTAEROSPACE.COM

ARC CP No.1358
December 1974

Garner, H. C.

533.693 :
533.6.013.422 :
533.6.048.2 :
533.6.011.35 :
533.693.9

A PRACTICAL APPROACH TO THE PREDICTION OF OSCILLATORY PRESSURE DISTRIBUTIONS ON WINGS IN SUPERCRITICAL FLOW

Brief consideration of current approaches to the prediction of unsteady wing loading in mixed subsonic and supersonic flow shows a wide variety of method and a clear need for economy in transonic aerodynamic calculations for flutter clearance in subsonic flight. In support of measurements of steady and oscillatory pressure distributions on a particular wing, an approximate theoretical treatment is devised in terms of non-linear steady surface pressures and linear oscillatory loading. The steady data are taken either from transonic small-perturbation theory or from the static experiments. The resulting theoretical or semi-empirical calculations can take account of stream Mach number, mean incidence, mode of oscillation, frequency and amplitude. Like the dynamic experiments, the theoretical and semi-empirical results show large differences between oscillatory chordwise load distributions under subcritical and supercritical conditions, especially in the recompression region where the large and rapidly changing amplitude and phase of the measured loading are reproduced qualitatively in the calculations. The method should provide an economical indication of the importance of non-linear flutter aerodynamics in the lower transonic regime.

ARC CP No.1358
December 1974

Garner, H. C.

533.693 :
533.6.013.422 :
533.6.048.2 :
533.6.011.35 :
533.693.9

A PRACTICAL APPROACH TO THE PREDICTION OF OSCILLATORY PRESSURE DISTRIBUTIONS ON WINGS IN SUPERCRITICAL FLOW

Brief consideration of current approaches to the prediction of unsteady wing loading in mixed subsonic and supersonic flow shows a wide variety of method and a clear need for economy in transonic aerodynamic calculations for flutter clearance in subsonic flight. In support of measurements of steady and oscillatory pressure distributions on a particular wing, an approximate theoretical treatment is devised in terms of non-linear steady surface pressures and linear oscillatory loading. The steady data are taken either from transonic small-perturbation theory or from the static experiments. The resulting theoretical or semi-empirical calculations can take account of stream Mach number, mean incidence, mode of oscillation, frequency and amplitude. Like the dynamic experiments, the theoretical and semi-empirical results show large differences between oscillatory chordwise load distributions under subcritical and supercritical conditions, especially in the recompression region where the large and rapidly changing amplitude and phase of the measured loading are reproduced qualitatively in the calculations. The method should provide an economical indication of the importance of non-linear flutter aerodynamics in the lower transonic regime.

Cut here

ARC CP No.1358
December 1974

Garner, H. C.

533.693 :
533.6.013.422 :
533.6.048.2 :
533.6.011.35 :
533.693.9

A PRACTICAL APPROACH TO THE PREDICTION OF OSCILLATORY PRESSURE DISTRIBUTIONS ON WINGS IN SUPERCRITICAL FLOW

Brief consideration of current approaches to the prediction of unsteady wing loading in mixed subsonic and supersonic flow shows a wide variety of method and a clear need for economy in transonic aerodynamic calculations for flutter clearance in subsonic flight. In support of measurements of steady and oscillatory pressure distributions on a particular wing, an approximate theoretical treatment is devised in terms of non-linear steady surface pressures and linear oscillatory loading. The steady data are taken either from transonic small-perturbation theory or from the static experiments. The resulting theoretical or semi-empirical calculations can take account of stream Mach number, mean incidence, mode of oscillation, frequency and amplitude. Like the dynamic experiments, the theoretical and semi-empirical results show large differences between oscillatory chordwise load distributions under subcritical and supercritical conditions, especially in the recompression region where the large and rapidly changing amplitude and phase of the measured loading are reproduced qualitatively in the calculations. The method should provide an economical indication of the importance of non-linear flutter aerodynamics in the lower transonic regime.

Cut here

DETACHABLE ABSTRACT CARDS

DETACHABLE ABSTRACT CARDS

This Document Provided by the Abbott Aerospace
TECHNICAL LIBRARY
ABBOTTAEROSPACE.COM

C.P. No. 1358

© *Crown copyright*

1976

Published by
HER MAJESTY'S STATIONERY OFFICE

Government Bookshops
49 High Holborn, London WC1V 6HB
13a Castle Street, Edinburgh EH2 3AR
41 The Hayes, Cardiff CF1 1JW
Brazennose Street, Manchester M60 8AS
Southey House, Wine Street, Bristol BS1 2BQ
258 Broad Street, Birmingham B1 2HE
80 Chichester Street, Belfast BT1 4JY

Government Publications are also available through booksellers

C.P. No. 1358

ISBN 011 470994 7